Cross-linking, morphology and properties in polymer blends and composites

Yasin Hamid, Ph.D.

Doctoral Thesis Summary

Tomas Bata University in Zlín

Tomas Bata University in Zlín
Faculty of Technology

Doctoral Thesis Summary

Síťování, morfologie a vlastnosti polymerních směsí a kompozitů

Cross-linking, morphology and properties in polymer blends and composites

Author:	**Yasin Hamid Ph.D.**
Degree programme:	P2808 Chemistry and Materials Technology
Degree course:	2808v006 Technology of Macromolecular Compounds
Supervisor:	prof. Ing. Petr Svoboda, Ph.D.
External examiners:	doc. Ing. Martin Obadal, Ph.D., doc. Petr Filip, CSc.

Zlín, April-2021

Published by **Tomas Bata University in Zlín** in the Edition **Doctoral Thesis Summary.**
The publication was issued in the year 2021

Key words in Czech: *Electromechanic, Irradiation, Thermal conductivity, Carbon fibre, EVA, EBC*

Key words: *Electromechanic, Irradiation, Thermal conductivity, Carbon fibre, EVA, EBC*

Full text of the doctoral thesis is available in the Library of TBU in Zlín.

ISBN 978-80-7454-998-4

Abstrakt:

Byly studovány tři elektricky vodivé kompozity obsahující uhlíkové plnivo: (1) ethylenvinylacetát (EVA)/uhlíková vlákna (CF), (2) ethylen-butenový kopolymer (EBC)/elektricky vodivé saze (CB) a (3) EBC/CF. Kompozity byly připraveny mícháním na dvouválci nebo v Brabenderu. Destičky byly připraveny lisováním. U kompozitů EVA/CF byl studován vliv ozáření elektrony při úrovních 60, 120 a 180 kGy. Studium obsahu gelu pomohlo při výpočtu parametrů Charlesby-Pinnerovy rovnice. Parametry G(X) = 3,78 a G(S) = 2,35 znamenají, že během ozařování elektronovými paprsky dochází k síťování i štěpení řetězců. Poměr parametrů G(X)/G(S) = 1,61 znamená, že u tohoto EVA kopolymeru převažuje síťování nad štěpením. Vyvolané změny mechanických vlastnosti při pokojové teplotě (25 °C) a při vysoké teplotě (150 °C) (kríp, napětí-deformace a frekvenční závislost) byly studovány pomocí dynamické mechanické analýzy (DMA). Vliv ozáření proudem elektronů byl nejlépe pozorován při 150 °C; došlo k systematickému poklesu krípu, zvýšení napětí při dané deformaci, zvýšení reálné části modulu pružnosti ve smyku G' a snížení ztrátového faktoru (tan delta). Experimentálně naměřené zvýšení modulu pružnosti v důsledku přídavku uhlíkových vláken bylo diskutováno pomocí Guth-Goldova a Guth-Smallwoodova modelu. Tvarový faktor L/D byl odhadnut přímým pozorováním pomocí světelné mikroskopie. Kompozity byly testovány na změny elektrického odporu během zatěžování různými silami. Byl vypočten měrný faktor, definovaný jako poměr relativní změny elektrického odporu k mechanickému prodloužení. Některé kompozity vykazovaly významné změny elektrického odporu během zatěžování v tahu, což naznačuje možnost budoucího využití těchto elektricky vodivých kompozitů jako senzorů deformace, které by mohly být použity např. jako umělé svaly v robotice.

Abstract:

Three electrically conductive carbon containing composites were studied: (1) ethylene vinyl acetate (EVA)/carbon fibers (CF), (2) ethylene-butene copolymer (EBC)/electrically conductive carbon black (CB) and (3) EBC/CF. The composites were prepared by mixing on a two-roll mill or in a Brabender. Sheets were prepared by compression molding. The influence of electron beam irradiation at levels 60, 120 and 180 kGy was studied for EVA/CF composites. Gel content study helped in calculation of the parameters in Charlesby-Pinner equation. Parameters G(X) = 3.78 and G(S) = 2.35 mean that both cross-linking and chain scission occur during e-beam irradiation. The ratio of the parameters G(X)/G(S) = 1.61 indicates that cross-linking prevails over the scission for this EVA copolymer. Room temperature (25°C) and high-temperature (150°C) mechanical properties (creep, stress-strain and frequency sweep) were studied by dynamic mechanical analysis (DMA). The influence of electron beam irradiation was best observed at 150°C; there was a systematic decrease in creep, increase in stress at given strain, increase in real part of shear modulus G' and decrease in loss factor (tan delta). The experimentally obtained increase in modulus due to the addition of carbon fibers was discussed with the help of Guth-Gold and Guth-Smallwood models. Shape factor L/D was estimated by direct observation by optical microscopy. The composites were tested for changes in electrical resistance during the stretching by various forces. Gauge factor, defined as the ratio of relative change in electrical resistance to the mechanical strain, was calculated. Several composites showed significant changes in electrical resistance during stretching showing a potential use of these electrically conductive composites as strain sensors that could be used for example as artificial muscles in robotics.

Table of Contents

List of Abbreviations

CB	Carbon Black
CF	Carbon fiber
DMA	Dynamic Mechanical Analysis
E	Modulus
EBC	Ethylene-butene copolymer
EVA	Ethylene-vinyl acetate
G″	Loss modulus
G′	Storage modulus
Gc	Shear modulus of the composite
Gm	Shear modulus of the gum
J(t)	Creep compliance
k	Sample specific pre-exponential factor
kGy	kilo Gray
$MgCl_2$	Magnesium chloride
n	Shear thinning exponent
PAN	Poly acrylonitrile
SiC	Silicon carbide
SoO_2	Silicon dioxide
T_g	Glass transition

$Ti(OBu)_4$	Titanium butoxide
$TiCl_4$	Titanium tetrachloride
$Zn\text{-}Cl_2$	Zinc chloride
η	Viscosity
η^*	Complex viscosity,
σ	Stress
ω	Oscillation frequency
Φ	Volume fraction of the filler
τ	Deformation

Introduction

Recently, there have been lots of polymer replacement interests instead of other materials like Metal, Wood, ceramics [5]. This because of the advantages that polymer offers over conventional materials like cost, easy to process, and productivity. [6]

To meet the high demands base on strength and stiffness for many applications, the polymeric materials must be reinforced like aerospace. Automotive, medical, chemical industry, electrical, construction, microelectronics, and sensors [7, 8]. Carbon fiber and glass fibers are more attractive in the academic and commercial fields due to their cost and functionality [7, 9-11].

There are two types of additives used in Polymer Composites. The reinforcing fibers in polymer composites are more responsible for their high stiffness and strength. That could satisfy with sufficient stress transfer to the matrix from fiber and vice versa, which can occur by suitable bonding between them [12]; Therefore, the properties and structure of the Fiber-Matrix play the primary role in both the physical and mechanical properties of Polymer Composites.

The most famous and ordinary fiber is carbon fiber, glass fiber, and amid family. The glass fiber has good tensile strength. However, it has low stiffness compared to other fibers. Nevertheless, due to limited recyclability and high-energy glass fibers requirements, they are still causing environmental problems. Because of trends toward environmentally friendly, most of the research focuses on using environmentally friendly fibers as alternatives to glass fibers.

Carbon fiber is widely used in the industry nowadays. Carbon-filled polymer composites have been popular due to their extensive utilization in various electronic equipment like temperature, pressure, dielectric, strain, gas, and biosensor materials.

Carbon fibers (CF) have become a critical reinforcing material in advanced composites because of their too high strength, stiffness, heat-resistance, and low weight. Fiber-reinforced polymer composites have a great interest due to their very high strength-to-weight and stiffness-to-weight ratios. These properties are significant in aerospace, engineering, marine industries, and automobile industries. The adhesion at the interface between matrix and fiber is an essential issue in controlling the composite properties. [13, 14]

An excellent interface between fiber and matrix can increase the stability and transfer the stress from matrix to fiber. However, chemical inertness and smooth surface of the fiber causes poor adhesion and lower enhancement in the properties of the composite. All these advantages can be combined and increase with a suitable matrix or achieve the excellent mechanical properties of composite parts built from both. [7, 14-17]

Fillers are mainly used in composites in two forms. They are mainly used in particles and short fibers, usually added to the matrix to enhance and increase the process's mechanical properties. Fillers' behavior in the composite mixture is affected by the particle size, distribution, surface at area shape, and surface chemistry. For example, Silicon carbide (SiC), which knows and ceramic material that compounds or silicon and carbon, could increase the abrasion resistance. Silicon carbon has unique physical properties, which enhance the chemical and mechanical properties. Meanwhile. It is resistant to high thermal, electron mobility, and excellent thermal conductivity.

Electrical properties can be affected by many fillers. For example, by adding conductive fillers, an electromagnetic shielding property can be built into plastics, which usually are poor electrical conductors. Carbon family fibers like carbon fiber,

Carbon nanotube, Carbon black, and graphite are mostly used as a fiber to improve the electrical and thermal conductivity and mechanical and physical properties.

Electrically conductive composites have been adequately prepared by adding an electrically conductive filler to polymeric materials. Several researchers have investigated various inorganic fillers such as carbon black [18], carbon nanotubes (CNTs) [19], SiO_2 Nanoclay [20]. For example, conductive composites with carbon black (CB) are attractive due to their applications in the automotive, pressure sensor, and gas sensor.

Several categories could affect the fillers' function in composites, such as the size, roughness, and aspect ratio. If the filler's characterization is with a low aspect ratio, there will be less change in basic properties than unfilled polymers. However, it could improve thermal resistance, Strength, and solvent resistance. Nevertheless, the impact resistance and shrinkage will often be less than the unfilled polymer. On the other hand, increasing the filler's aspect ratio up to 25, the filler can be characterized as a fiber. Fiber reinforcements will significantly affect the properties of the mixtures to which they are introduced. The fiber impact strength would increase, mainly if many fibers are oriented in the one direction in which a considerable difference is observed between the unfilled and filled polymer's modulus. Besides, increasing the aspect ratio could decrease the shrinkage in the order of the fiber.

Previously, Carbon fibers were made from natural cellulosic fibers such as linen or cotton for thousands of years. Nevertheless, it was Thomas Edison who, in 1978, produce carbon fiber from bamboos and cotton in his research for lamp filaments. In the meantime, the late 1950s, carbon fiber was interesting for scientists once carbon fiber was produced from synthetic rayon is in textile forms for high-temperature missile applications. [21]

Several studies have been done about the mechanical and electromechanical study of composites with conductive fillers [9, 22-26]. The fast development of smart sensors has contributed to smart elastic strain sensors. However, to date, the low stretch-ability and sensitivity of conventional metals or inorganic semiconductor-based strain sensors have restricted their application in this field to some extent [1-4]. Slobodian et al. [27] reported that the addition of multi-wall carbon nanotube (MWNT) up to 20 wt.% to poly (methyl methacrylate) (PMMA) could increase the conductivity up to 100 times. Spherical particles like Carbon Black in polymer/carbon black composites exhibit percolation threshold, frequently up to 15–25 wt.%. However, lower values were also published. D'Aloia et al. [28] investigated that graphene's addition leads to an increase in the graphene-thermosets polymer's electromechanical and mechanical properties. As the graphene concentration increases, the graphene-polymer composite undergoes an insulator-to-metal transition due to the conductive filler presence inside the matrix. It is also reported that the addition of carbon nanotube to SEBS elastomer could increase electrical resistance. At the same time, the sample is stressed and decreasing when the sample recovers to initial deformation. Furthermore, it has been shown that the sample leads to stable after some aging cycles [29]. Yang et al. [30] investigated the resistance response of CNT/ graphene RTV silicone rubber composites under static and dynamic cyclic loading. It is observed that CNT/graphene RTV silicone rubber composites exhibited a stable and reproducible resistance response under dynamic cyclic loading, indicating that they have potential applications in continuous monitoring. Mostly, strain sensors are based on piezoresistive materials, for example, those materials for which an applied strain, ε, results in a resistance change. Commonly, the gauge factor is measured at low strain, which is most metals is small in the range 2 for Nichrome V to 4.8 for Platinum [31]. However, composite strain sensors based on polymers filled with conductive fillers, like multiwalled carbon

nanotubes [32] and carbon nanotube[33, 34], can gauge high gauge factors. Piezoresistive materials resistance increases with increasing tensile strain as they have positive gauge factors because interparticle intersections dominate the piezoresistance in composites, leading absolutely to the Gauge factor higher than 0. A small number of materials with negative gauge factors [35]; polymer fibers coated with conducting polymers have demonstrated small negative gauge factors due to chain alignment effects.

Creep study of isotactic polypropylene (iPP)-based graphene nanocomposites used to evaluate the load transfer efficiency by Gaska [36] et al. they have investigated that significant increase of Young's modulus with increasing filler content which indicates reasonably good dispersion and adhesion between isotactic polypropylene (iPP)-based graphene nanocomposites the and the filler content indicates reasonably good dispersion and adhesion between the iPP and the filler. Wang [37] et al. reported the same results for numerical analysis using the Finite Element Method used for unidirectional fibrous polymer matrix composites' computing material properties. Srivatsan and Sreekanth [38] investigated the experimental characterization of dynamic mechanical properties of carbon fiber-reinforced composite with sandwich configuration. The addition of carbon fiber up to 40 wt.% will increase the loss modulus and tan delta curve as the frequency increases. They also indicated that Carbon exhibiting high storage modulus due to its atomic structure directly indicates young's modulus. Sabet et al. [39] studied the impacts of graphene inclusion on the mechanical, electrical, and low-density polyethylene. They reported that while the addition of 3 wt.% of graphene had a significant impact on the performance and improvement of LDPE's electrical characteristics, which is because of the spreading of graphenes in LDPE, which makes to extend more conductive networks. The polymer composite's viscosity is rasing from 120.1 to 195.4 kPa because of the significant interaction between the

filler and matrix that obstructed the movement of macromolecular polymeric links. Consequently, graphene has an excessive surface area and nanoscale fat surface that renders it generate resilient interfacial connections with LDPE and significantly affects an excellent consequence of LDPE's chain movement. It has been communicated that the mechanical properties and dynamic properties can be enhanced by entering the e-beam irradiation due to enhancing the filler to matrix interaction, shown in swelling resistance studies [40]. Introducing carbon fiber or nanotube to EVA can improve the modulus and the composite's tensile strength.

Polymer material radiation processing involves ionizing radiation of polymer treatment to enhance their chemical and mechanical properties. During the ionizing irradiation, polymers can cross-link, be grafted, or degrade. [41, 42] Mateev et al. investigated the effect of e-beam irradiation on the gel formation process of EVA/PE films in range 40-250kGy when the significant change in gel content occurred in range 40-170kGy [43]. This fact and our experience from our previous experiments [44] influenced our range of e-beam radiation, being this time 60, 120, and 180 kGy. Electron beam (EB) irradiation on EVA/CF composite has been used in this study, and a variety of fiber concentrations has been investigated.

In this study, the electromechanical and rheological properties of electrically conductive carbon black (CB) on ethylene Butene copolymer have been investigated. The electrical conductivity of CB is studied both in terms of creep and filler content. The mechanical properties of EVA/CF composite under EB irradiation have been investigated in detail. Testing mechanical properties was done at room temperature (25 °C) and 150°C. We are presenting only high-temperature results since they better reflect the influence of e-beam cross-linking.

The amorphous polymer chains are held together by crystal lamellae and covenant bonds (from cross-linking). However, at 150°C, only the chemical cross-linking has the amorphous chain together.

2. Electron beam irradiation

Electron beam irradiation was applied at room temperature in BGS Beta-Gama-Service Gmbh, Germany. The process is controlled not to surpass 50 °C. The source of radiation is toroid electron accelerator Rhodotron (10 MeV, 200kW). The irradiation is applied in a tunnel on a moderately moving conveyor with the irradiation dosage ranging from 60 to 180 kGy (30 kGy per pass) with 3m/min belt speed and 10 mA with 78 cm sample distance from the scanner for 2-second irradiation.

1.1. Optical microscopy

Carbon fiber's dimensions are evaluated with optical microscopy using an Olympus RX41 microscope (Tokyo, Japan) to calculate the aspect ratio (L/D length over diameter) of carbon fiber in the composite.

1.2. Gel content

The gel contents of electron-beam cross-linked EVA samples were obtained by calculating the insoluble cross-linked material after extracting the solvent according to ASTM D2765-01. A small amount of cross-linked material (about 0.15 g) was wrapped in a stainless steel cage and placed in boiling xylene solvent for 6 h with 1 wt.% of an antioxidant. The sample was weighted after the evaporation of the solvent. Finally, the gel content was calculated as the percent ratio of the final weight to the sample's initial weight multiplied by one hundred.

To calculate the starting gel dose and the radiation chemical yield of cross-linking and scission, the widely accepted Charlesby-Pinner equation was used

$$s + \sqrt{s} = \frac{p_0}{q_0} + \frac{1}{q_0 P_n D} \quad (1$$

$$In\ plot \quad s + \sqrt{s} \quad vs. \ \frac{1}{D}: \quad intercept = \frac{p_0}{q_0}, \ slope = \frac{1}{q_0 P_n}$$

Where p_0 and q_0 are the chain scission and cross-linking density per unit dose in kGy^{-1} respectively, Pn is the average number degree of polymerization before irradiation, and D is the irradiation dose in kGy

1.3. Electric resistance

The electrical resistance changes of change in strain-relaxation cycles were analyzed with precise weight using the two-point technique. The test was done using various forces (1,2,3,4,5 N) for 5 minutes to measure the strain and electric resistance change in time. The change of resistance was measured with the Vernier LabQuest Interface System (VLQIS) connected to the Differential Voltage Probe and the Wheatstone bridge with sampling frequency 200Hz.

1.4. Dynamic Mechanical Analysis (DMA)

METTLER Toledo Switzerland performed the dynamic mechanical analysis. Samples with dimensions of 11 × 11 × 0.5 mm were tested for creep-relaxation, stress-strain, and frequency sweep. The stress-strain was performed in a force range 0 to 2 N with a 0.4 N/min force rate at 150C. The creep relaxation was measured in three steps. At first, the sample is placed in the DMA machine for 1 min at 150 °C under 0.05 N. The sample was then under the creep test for 5 min at 150 °C under 1 N force. Finally, the force dropped to 0.05 N for 5 min at 150 °C for relaxation. The frequency sweep test was done at 150 °C with a preload force of 0.1 N in the frequency range 0.1 to 100 Hz by 10 steps per decade with 10 μm displacement.

1.5. Thermal conductivity

The process of measurement and the instrument are explained below. At first, the 5 cm diameter central brass cylinder (CBC) is bound to reach t2 =45°C with another chamber's assistance related to an indoor water regulator by elastic hoses with a water thermostat with 0.1°C accuracy. This takes about 3 minutes to reach a suitable temperature. Then the hot chamber is quickly removed. The sample with a 5 cm diameter is placed on top of CBC with a second brass cylinder on the top with a weight of 100g, which is connected to a second water thermometer with the temperature set to 25° C.

The heat transfer from the hot CBC to the cold cylinder while going throw the sample. The CBC temperature is reducing quickly. The CBC data is collected every 5 s for 30 min by a thermocouple associated with a National Instruments information obtaining hardware (NI USB-9211A, Portable USB-Based DAQ (Data Acquisition)) for Thermocouples software and following to the computer using the USB port. (1) The data was analyzed using LabVIEW signal Express 2.5.

2. Materials

2.1. Long Carbon Fiber

The fiber is produced by treating an acrylic fiber precursor with pyrolysis, surface treatment, and sizing processes. Each bobbin of Torayca (Toray Carbon Fibers America) from Japan carbon fiber is protected against dust and packed in the container to prevent damage during transportation. This never twisted fiber is used in the high tensile application. The specification of fiber is given in table 1.

Table. 1. Carbon fiber properties

Tensile Strength	2,450 MPa

Tensile Modulus	125 GPa
Strain	2.1%
Density	1.8 g/cm^3
Filament Diameter	7 μm

2.2. Carbon Black fiber

The conductive Carbon Black (KETJENBLACK EC300J) with the composition of 10 wt.% polycarbonate with 99.95% purity is used for this study were purchased from Akzo Nobel Polymer Chemicals Ltd. Shanghai, PR China, with a bulk density of 0.125-0.145 g/cm^3 and apparent density of 2.26 g/cm^3, pore volume (DBP) 310-345 ml/100 g and 3.9Ω·cm. This CB is mainly used as an electro-conductive filler used in resin compounds, electro-conductive battery materials, paint, colorant, and toner.

2.3. Ethylene-vinyl acetate (EVA)

Ethylene-vinyl acetate with trade name Supreme Ultra FL 00328 was used. ExxonMobil Chemical Belgium supplied it (Antwerp Belgium) the melt flow index (MFI) is 3.0 g/10 min and density 0.951 g/cm^3; with 28 wt.% of vinyl acetate.

2.4. Ethylene-Butene Copolymer (EBC)

Ethylene-butene copolymer (ENR 7467) was purchased from DOW Engage® chemical company in the USA with specific properties like ultimate tensile strength 2 MPa, tensile elongation of 600%. The melt flow index (MFI) is 1.2 dg/min and 0.862 g/ cm^3.

2.5. Preparation of materials:

Ethylene-vinyl acetate and Ethylene butyl copolymer with carbon fiber were mixed and homogenized with different concentrations (5, 10, 15, 20, 25 wt.%) using a two-roll mill at 150 °C for 5 min. A sheet with a thickness of 0.5 mm was prepared by compression molding at 150 °C and 10 MPa for 5 min preheating and 5 min pressing. Finally, the cold press was used for 10 min with 10 MPa pressure. In the end, the prepared samples were cut into the dumbbell shape for the creep test.

The same process is performed for Ethylene butyl copolymer and carbon black.

2.6. Electron-beam irradiation

Electron-beam irradiation was applied at room temperature in BGS Beta-Gama-Service Gmbh, Germany. The process was controlled not to surpass 50 °C. The source of radiation was toroid electron accelerator Rhodotron (10 MeV, 200kW). The irradiation was applied in a tunnel on a moderately moving conveyor with the irradiation dosage ranging from 60 to 180 kGy (30 kGy per pass) with 3 m/min belt speed and 10 mA with 78 cm sample distance from the scanner for 2-second irradiation.

2.7. Dynamic mechanical analysis (DMA)

METTLER Toledo Switzerland performed the dynamic mechanical analysis. Samples with dimensions of 11×11×0.5 mm were tested for creep-relaxation, stress-strain, and frequency sweep. The stress-strain was performed in a force range 0 to 2N with a 0.4 N/min force rate at 150 °C.

The creep relaxation was measured in three steps. At first, the sample was placed in the DMA machine for 1 min at 150°C under 0.05 N. The sample was then under the creep test for 5 min at 150 °C under 1N force. Finally, the force dropped to 0.05 N for 5 min at 150 °C for relaxation.

The frequency sweep test was done at 150 °C with a preload force of 1 N in the frequency range 0.1 to 100Hz by 10 steps per decade with 10 μm displacement. Higher frequency than 100 Hz is not recommended as all the specimen sizes except the one with 1 mm thickness are not useful due to their higher demand of displacement which the piezoelectric actuator is not capable of providing (2)

2.8. Gel content

The gel contents of electron-beam cross-linked EVA samples were obtained by calculating the insoluble cross-linked material after extracting the solvent according to ASTM D2765-01. A small amount of cross-linked material (about 0.15 g) was wrapped in a stainless steel cage and placed in boiling xylene solvent for 6 h with 1 wt.% of an antioxidant. The sample was weighted after evaporation of the solvent. Finally, the gel content was calculated as the percent ratio of the final weight to the sample's initial weight multiplied by one hundred.

2.9. Optical microscopy

Dimensions of carbon fibers were evaluated by optical microscopy using an Olympus RX41 microscope (Tokyo, Japan) to calculate the aspect ratio (L/D length over diameter) of carbon fibers in the composite.

2.10. Size-exclusion chromatography

The molecular weight measurement was performed at 160 °C on a Polymer Laboratories PL 220 high-temperature chromatograph (Polymer Laboratories, Varian Inc., Church Stretton, Shropshire, England) equipped with three 300 mm x 7.5 mm PLgel Olexis columns and a differential refractive index detector. 1,2,4-trichlorobenzene (TCB) was used as eluent, stabilized with butylhydroxytoluene (BHT) (Ciba, Basel, Switzerland) as an antioxidant. A mobile phase flow rate of 1 mL min^{-1} was used, and the volume of 200 mL was injected. The sample was

prepared to a concentration of 0.5 mg mL^{-1} in TCB. Narrowly distributed polyethylene standards (Polymer Standards Service GmbH, Mainz, Germany) were used for calibration purposes.

2.11. Electric resistance

For electrical characterization, several methods are used. The two-point probe method using a digital multimeter and four-point probe method using Hall effect measurements is more common(3). However, due to four-probe measurement limitations during the starching, the change EBC/CB's electrical resistance change in strain-relaxation cycles was analyzed with precise weight using the two-point probe technique. Two single-terminal electrodes are attached to the surface of the conductive structure called the two-point probe technique. A DC or AC source current is then connected through the two electrodes, and the subsequent voltage over the same electrodes is estimated. The electrical resistance between these two electrodes is then determined, according to Ohm's law.

To increase the results' reliability, copper plates used as electrodes were attached to the sample, dissolved the backing adhesive, flooded into butanone solution, and then washed using tap water. After drying and cleaning copper plates, the pellets were sandwiched with upper and lower Ag's electrodes using silver paint around the surface of dumbbell specimens. The test was done using various forces (1, 2,3,4,5 N) for 5 min to measure the strain and electric resistance change in time. When the samples were ready, an electrical circuit powered by a DSC power source was applied to the DC source was used for the tests for its simplicity. However, it is worth to mention that in reality, 1 kHz is commonly used to prevent polarization inaccuracy. The change of resistance was measured with the Vernier LabQuest Interface System (VLQIS) connected to the Differential Voltage Probe and the Wheatstone bridge with sampling frequency 200Hz.

3. Influence of carbon fibers on ethylene-vinyl acetate (EVA)

The influence of carbon fibers and radiation on shear stress creep compliance, and frequency sweep of ethylene-vinyl acetate (EVA) was investigated by dynamic mechanical analysis. The addition of carbon fiber into EVA leads to a significant increase in shear stress (see Figure 12). This behavior is similar to the one reported by Das *et al*. (4).

The shear stress of the EVA composites with a content of 20 wt.% of carbon fiber has the highest value. In contrast, the pure EVA has the lowest shear stress at the same shear strain (such as at 0.10 strain, the values are about 0.004 and 0.007 MPa for 0 and 20 wt.% of CF, respectively), due to the improved interfacial action (5). Hamid *et al*. reported that fiber could significantly improve stiffness by hindering the movement within the matrix (6).

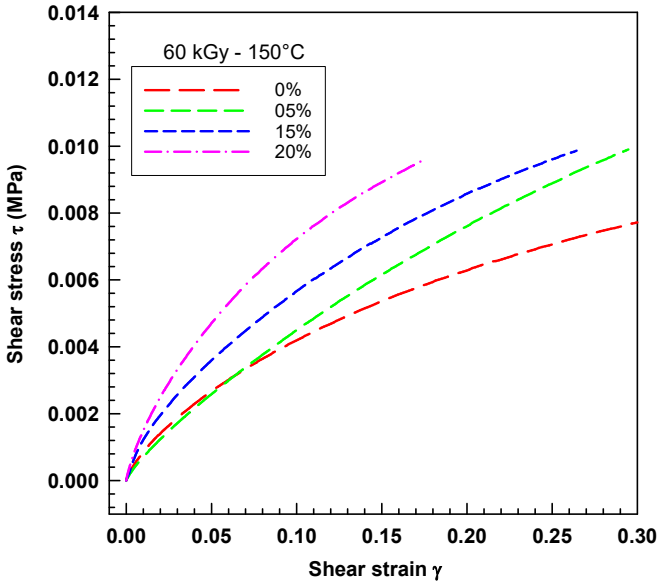

Fig. 1. Shear stress-strain curves of EVA/CF composites

The increase of shear modulus as a function of increasing CF content is illustrated in Figure 1. The highest values of G' were found for the sample irradiated by 180

KGy. These results are in agreement with other scientists. An increase in G' due to an increasing volume fraction of carbon nanotubes was reported, e.g., by Potschke *et al*. (7). An increase in G' values at 0.1 rad s^{-1} due to increasing e-beam radiation for ethylene-octene copolymer was reported, e.g., by Poongavalappil *et al.* (8).

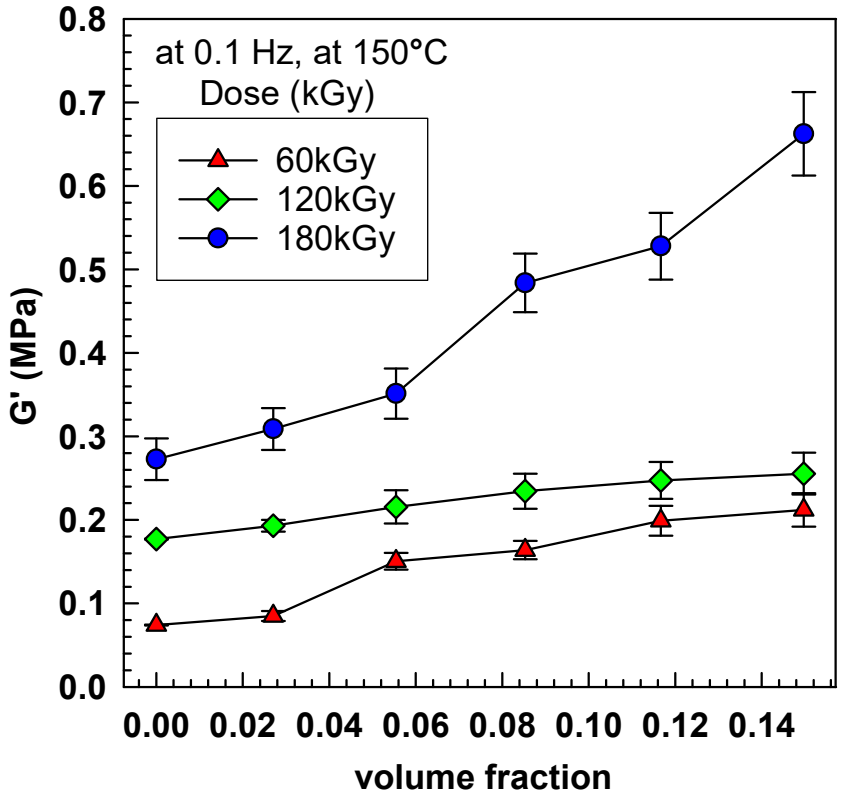

Fig. 2. Experimental relative G' at 150 °C at frequency 0.1 rad/s

To calculate the relative G' increase, it is necessary to calculate the fiber's volume fraction in the composite.

The volume fraction is calculated while the densities of CF and EVA 328 are 1.80 g/cm^3 and 0.951 g/cm^3, respectively.

Densities of the composites and volume fraction are listed in Table 2. These values are in a good agreement (within ±3%) to the experimentally obtained values (by pycnometer).

Table 2. Shear modulus in Experimental, Guth- Smallwood for spherical and non-spherical filler equation

Wa	**Φa**	**Density (g/cm^3)**	**Experimental at 0.1 Hz**	**G =Gm (1+ 2.5Φ +14.1Φ2)**	**Gc =Gm (1 +0.67 f Φ +1.62f 2Φ2)**
0	0	0.951	0.074	0.074	0.074
0.05	0.02705	0.97	0.0849	0.07977	0.1100
0.1	0.05545	1	0.1505	0.08747	0.1847
0.15	0.08528	1.02	0.1638	0.09737	0.3040
0.20	0.11667	1.05	0.1990	0.10979	0.4748
0.25	0.14974	1.08	0.2119	0.14974	0.7044

The volume fraction, the density of each composite, experimental (see Fig.3), Guth – Gold for spherical, and Guth-Smallwood for non-spherical particles are calculated, as shown in Table 2. To illustrate the modulus of EVA-CF composite, the aspect ratio of carbon fiber should be determined.

Figure 3 shows the comparison between the experimental modulus with Guth-Gold for spherical and Guth-Smallwood for non-spherical particles. It indicates that the non-spherical Guth-Smallwood is closer to the experimental data at lower concentrations; however, the Guth-Gold model is closer at higher concentrations.

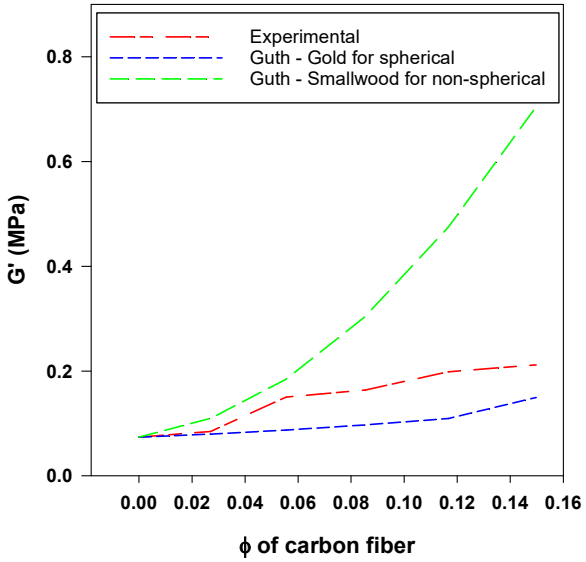

Fig. 3. Prediction of modules with Guth- Smallwood for spherical and non- spherical filler vs. experimental

The correlation of experimental increase in modulus with theoretical predictive models was well illustrated, e.g., by Mandal *et al*. (9).

The statistical data of the aspect ratio for EVA/CF composite are shown in Figure 4b. This data was obtained from various electronic microscope photographs of EVA in Fig.15a having different CF contents, i.e., 5-20 wt.%.

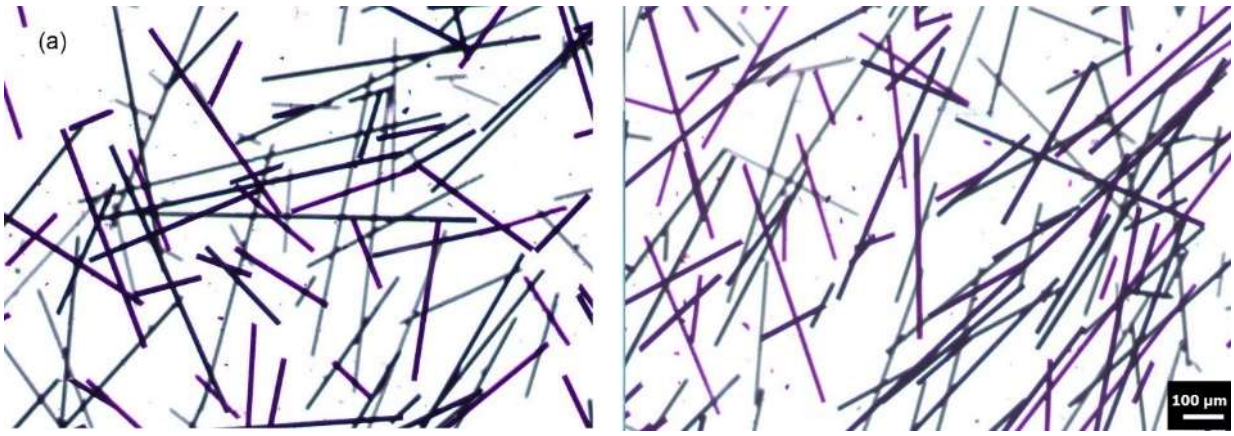

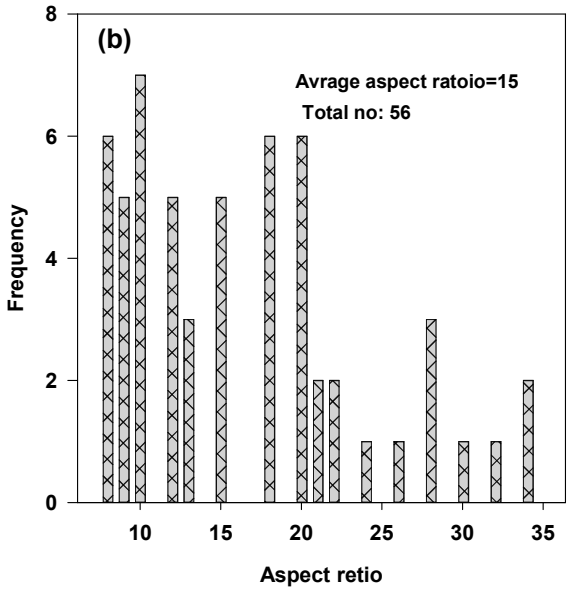

Fig. 4. a) Optical microscope image of EVA-CF, b) Histograms of the aspect ratio of carbon fiber in EVA-CF composites

The effect of irradiation dose on shear stress at 0.03 shear strain is visible in Figure 5 b. It is also common throughout the rubber industry to observe M100 modules and M300 of the modulus (at 100 and 300% elongation), and our choice was the stress at 0.03 shear strain. The graph indicates that EVA with a higher dose exhibited higher shear stress because EVA with a higher dose contains more radiation cross-links than a lower dose. It was observed that the shear stress of EVA with 5 wt.% of carbon fiber was following an exponential rise with R2=0.999 regression. As demonstrated in Figure 5 a, an addition of CF fiber with a higher radiation dose can enhance the shear stress, since CF as a filler and cross-linking can improve the stiffness by restricting the matrix (10, 11). Improvements in physical and mechanical properties of electron beam irradiation cross-linked EVA foams were also reported by Rezaian *et al*. (12). Mechanical changes of electron-beam irradiated EVA film were reported by Matsui *et al*. (13).

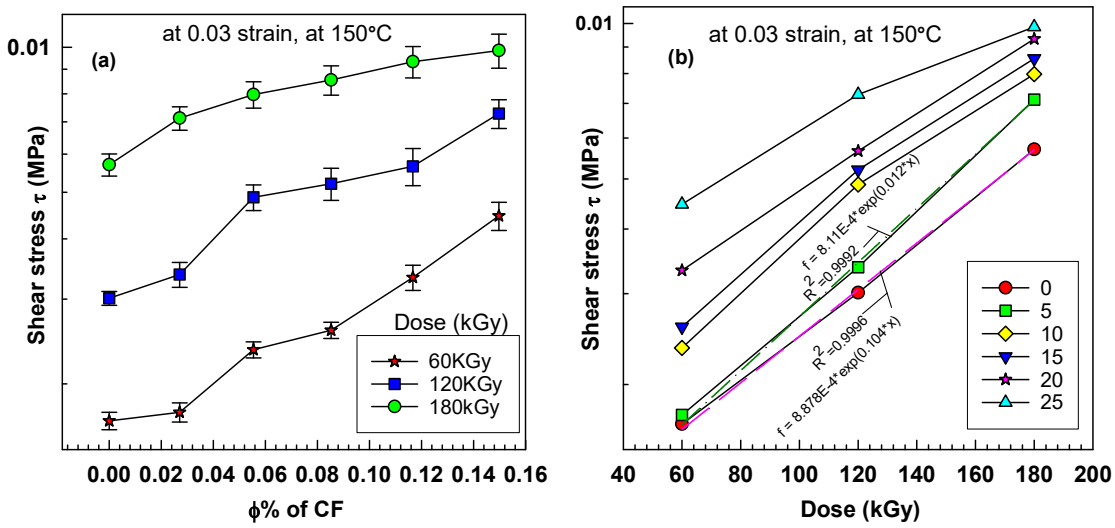

Fig. 5. a) Shear stress vol. fr. of *CF b) shear stress–dose curves of EVA/CF composites*

The development of creep in time is shown in Figure 6a. The addition of carbon fiber to EVA causes a reduction of the creep. It indicates that the addition of 20 wt. % of CF caused almost three times lower creep compared to pure EVA. The graph also shows that the creep is decreasing with the addition of carbon fiber and the rate of the creep (slope) decreases from 26 to 11 for pure EVA and 20 wt. % of carbon fibers, respectively. Figure 6b suggests a systematic decrease in creep with increasing content of the CF fibers after 5 min and after recovery observed after 10 min. Our results follow the trend of other researchers. Creep reduction due to Nano fillers' addition was reported, e.g., by Shokrieh *et al*. (14).

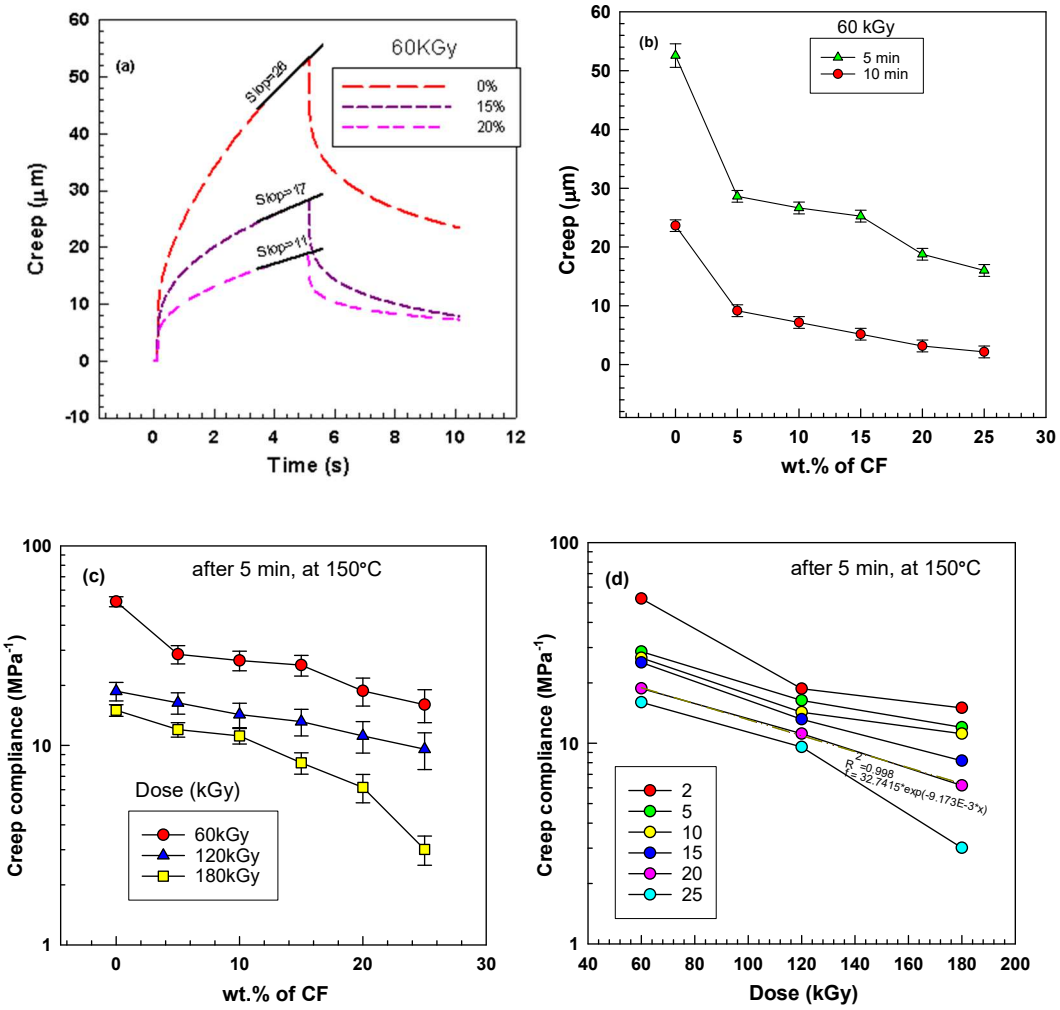

Fig. 6. a) creep–time b) creep (recovery)–wt. % curves of EVA/CF composite at 150 °C as a function of. c) wt. % of CF and d) dose (kGy) after 5 min.

Figures 6 c,d show the sensitivity of creep to CF content and radiation dose. The graph (Figure 17d) indicates a significant decrease in creep with a radiation dose (kGy). It shows that EVA composite with a dose of 180 kGy has nearly seven times lower creep compared to a dose of 60 kGy, which is caused by cross-linking. We have found an exponential decrease in creep compliance with increasing radiation levels in our previous study of the ethylene-octane copolymer (15). Creep reduction with an increasing level of cross-linking (by the addition of peroxide) was also reported by Theravalappil *et al*. (16).

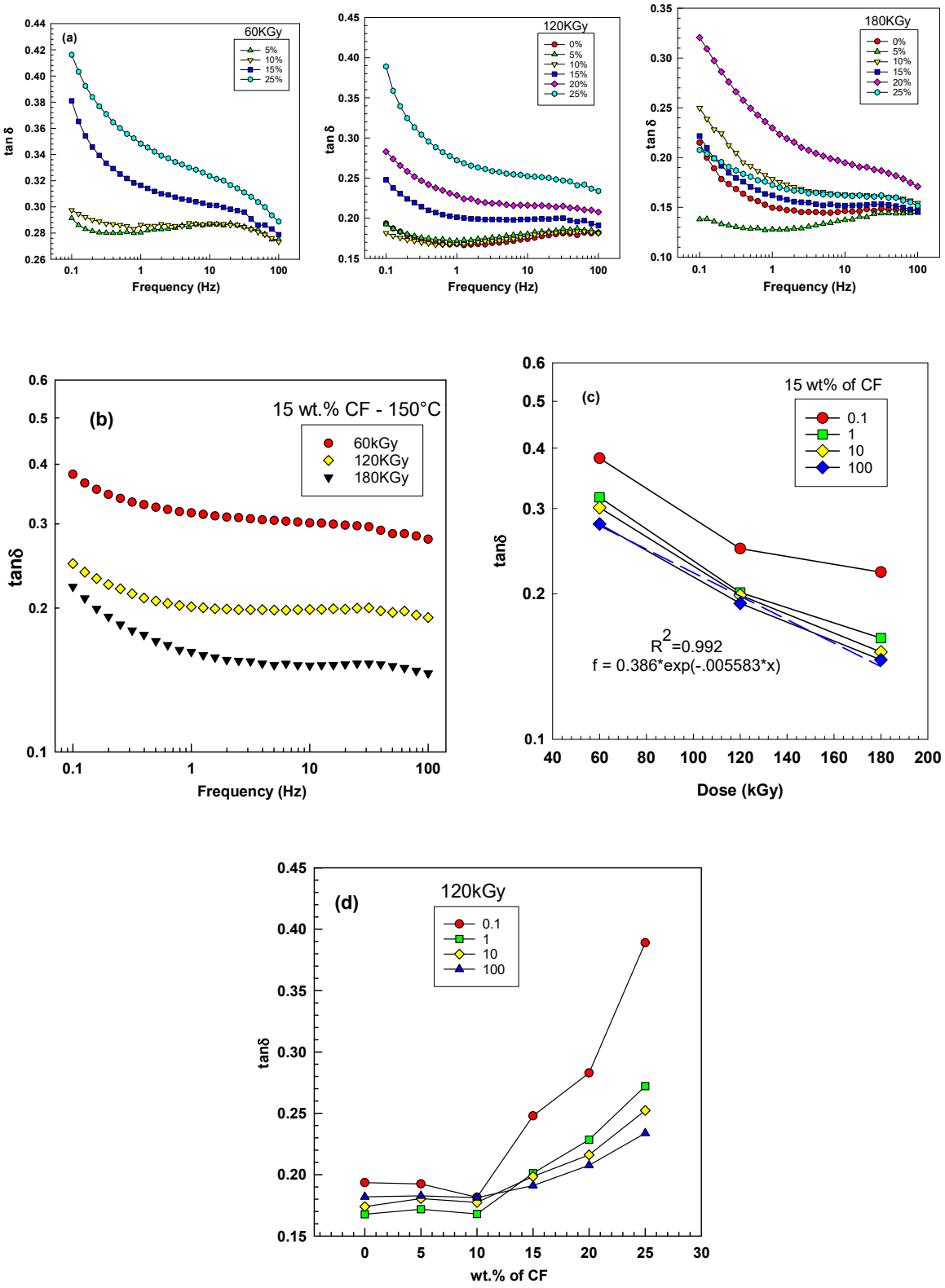

Fig. 7. tan δ at 150 °C. a, b as a function of frequency, c)Dose 0.1 rad/s, d) of CF content

Figure 7 shows the tan δ vs. frequency, dose, or CF content. The graph indicates that the addition of fiber to EVA will increase the tan δ. The tan δ for EVA composite (120 kGy) with 25 wt.% CF content is nearly 0.4, while the pure EVA is around 0.2, followed by 0.25 and 0.3 for 15% and 20%, respectively. A decrease of tan δ value with increasing cross-linking levels due to the addition of peroxide was reported, e.g., by Poongavalappil *et al*. (17).

Tan δ values have dropped by raising the radiation level from 60 kGy to 180 kGy. That is caused by an increase in molecular weight, which hinders the free flow of the material. It is also evident that the tan δ of the composites decreases significantly with increasing frequency, as shown in Figure 7a and b. The influence of frequency on the tan δ is complex. The chain motion can be restricted with the change of the external force, and the internal friction is low at low frequency; so, the tan δ is low. While in our cross-linked EVA system, the CF has caused an increase in tan δ McNally *et al*. (18) reported a decrease in tan δ values due to carbon nanotubes' addition in an uncross-linked PE. Figure 7c indicates the tan δ change with the dose at all frequencies. It shows that with an increase of the dose, tan δ is decreasing for all frequencies.

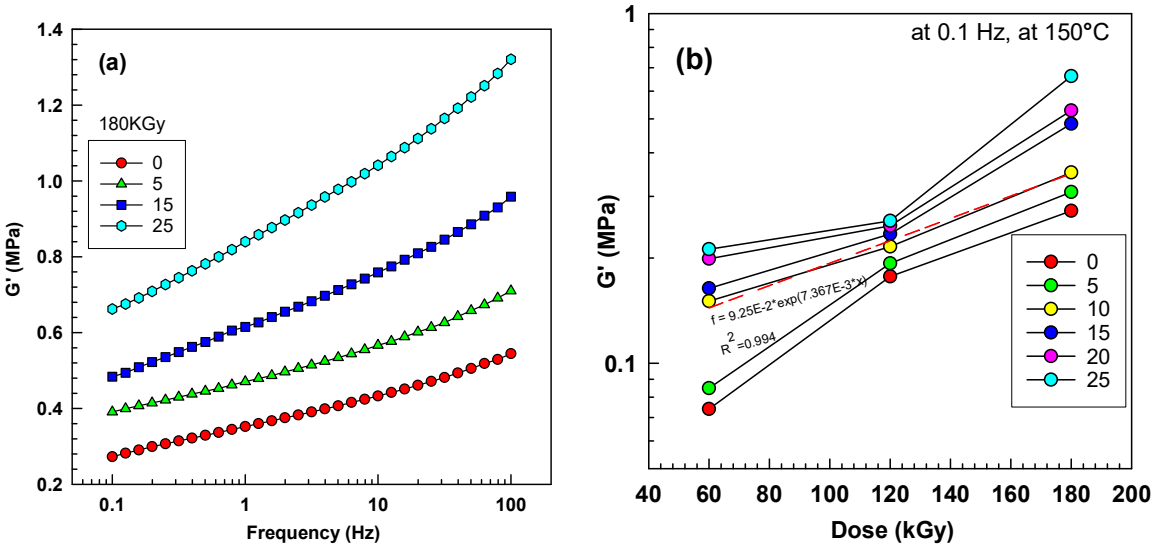

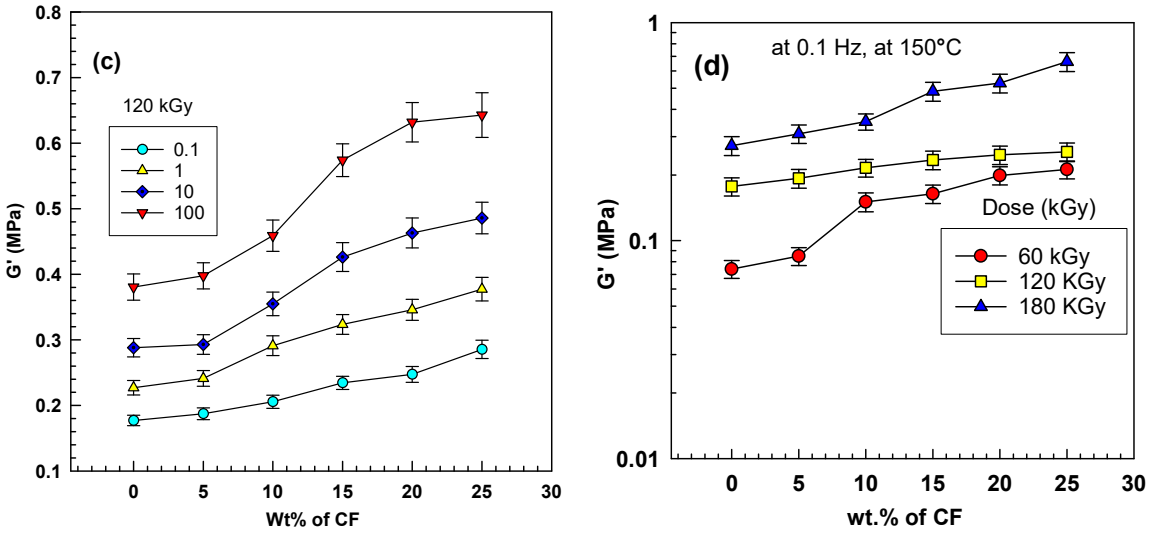

Fig. 8. Shear modulus (real part) G' at 150 °C. a, b as a function of frequency, c and d for frequency 0.1 rad/s as a function of c)dose, d) carbon fiber content

Figure 8 shows the G' increases after irradiation. The increase of G' was observed in the irradiation dose-ranging 60-180 kGy. For the EVA 25 wt.% of carbon fiber, the increase of G' was higher. The highest increase of G' was found for EVA 25 wt.% of carbon fiber (in the range 20-67 kPa). For the range of 60, 120, and 180 kGy, the G' values for pure EVA were 8, 17, and 28 kPa, respectively, and for EVA 15 wt.% of carbon fiber, they were 16, 23, and 43 kPa. An increase in G' due to the cross-linking was reported, e.g., by Mussatti and Macosko (19).

It has also been observed that fiber has an increased influence at a higher frequency. An increase in G' value due to the increasing level of carbon nanotubes was reported, e.g. by Potschke *et al*. (7, 20), and also due to the increasing level of graphene, e.g. by Kim and Macosko (21) or by Varghese *et al*. (22).

Calculation of G parameters according to Charlesby-Pinner equation (23, 24)

To be able to calculate Charlesby-Pinner parameters, it is necessary to have data on molecular weight and data of gel content for various levels of irradiation.

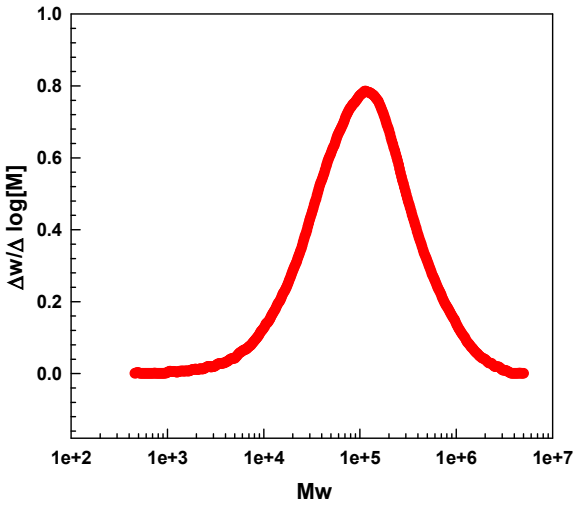

Fig. 9. The molecular weight distribution of EVA

Figure 9 depicts the EVA molecular weight distribution using gel permeation chromatography (GPC). The graph shows that EVA's molecular weight in this study is between 300 to 5000000 g/mol. The peak position is around 100000 g/mol. The results from the GPC test are listed in Table 3.

Table. 3. GPC results of EVA 328

Sample Name	Mp	Mn	Mw	Mz	Mz+1	PD
	g/mol					
EVA 328	113000	43400	196000	625000	1286000	4.5

Figure 10 shows that increasing the radiation dose to 60 kGy caused the generation of an insoluble 3D network with gel content being 72 wt.%. In the radiation range 60–180 kGy, the gel content is increasing only moderately, as shown in Figure 10 for 72%, 81%, and 89%, respectively, which could be ascribed to the increase in molecular weight and cross-linking.

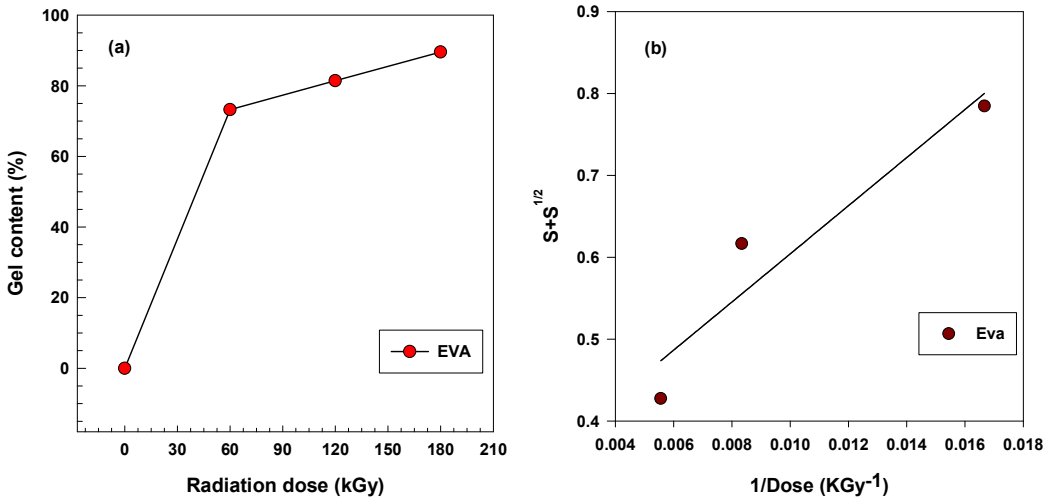

Fig. 10. a) Gel content results for three radiation cross-linked EVA

b) Charlesby–Pinner analysis

These results are in good agreement with Sharif *et al*. (25), who studied radiation effects on LDPE, EVA, and their blends. Figure 10b was used in Charlesby-Pinner calculation, as shown below.

Table. 4. Calculation of Charlesby-Pinner parameters

wt.% of vinyl acetate	**wt. fraction of vinyl acetate**	**wt. fraction of ethylene**	**molar fraction of vinyl acetate**	**molar fraction of ethylene**	**M_{ET-VA}**	**M_n**	**P_n**
28	0.28	0.72	0. 8875	0.1125	34.58	43400	1255

slope	p_0/q_0	q_0	p_0	G(X)/G(S)	G(X)	G(S)
29.38	0.3103	2.7121E-05	8.4156E-06	1.6113	3.7797	2.3456

All the essential parameters are listed in Table 4. Parameters G(X) =3.78 and G(S)=2.35 mean that both cross-linking and chain scission occur during e-beam irradiation. The ratio of the parameters G(X)/G(S) =1.61 indicates that cross-linking prevails over the scission for this copolymer. The ratio G(X)/G(S)=1.61 is comparable to our previous results on ethylene-octene copolymer with 30 wt.% of octene (26) when the ratio was 1.77.

4. Influence of Carbon black on ethylene butene copolymer (EBC)

The influence of Carbon black and force on shear stress, creep compliance, frequency sweep, and electromechanical study of the ethylene butene copolymer (EBC) was investigated by Dynamic Mechanical Analysis (DMA).

Figure 11 indicates the effect of force and CB content on creep after 5 min of EBC/CB composite. The creep of the composites with a content of 25 wt.% of carbon fiber has the lowest value for almost four times compared to the pure EBC, which has the highest creep. Additionally, increasing the force could increase creep due to the improved interfacial action between the copolymer and the fiber (5). Moreover, stiffness could be improved by fiber's addition by hindering the matrix material (6).

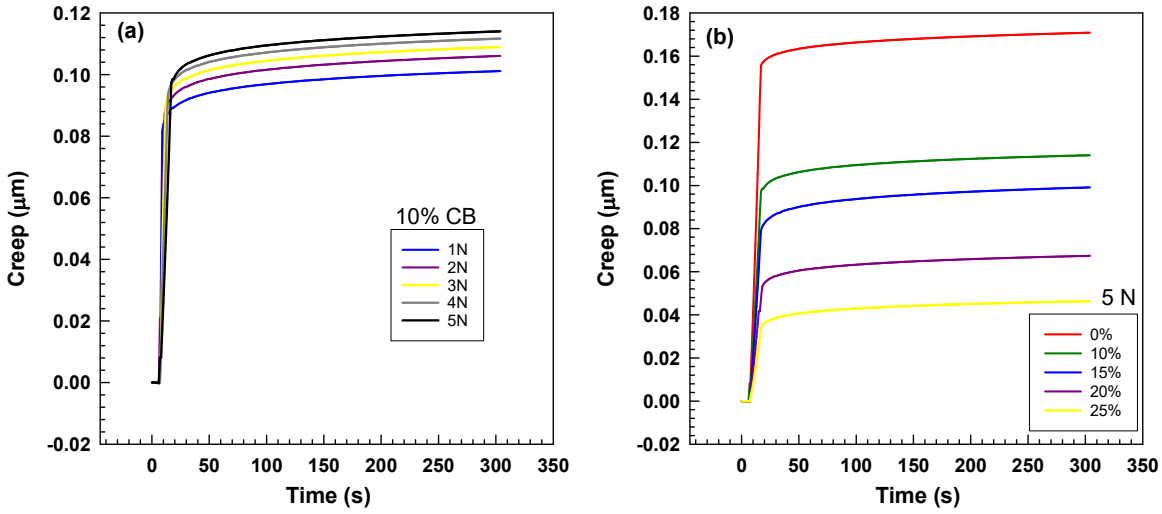

Fig. 11. creep–time for a) 10 wt.% CB b) 5N curves of EBC/CB composite at 25 °C for different concentration and stress

It shows that elongation (ε) significantly decreased by increasing the CB content up to 20 wt.%. On the other hand, there is not much difference from 20 wt.% to 25 wt.% as the fiber looks well dispersed, and the filler covers the matrix. It also indicates that increasing the force up to 5 N could increase elongation six times due

to the butene polymer composite's rubber behavior. The creep compliance graph shows that the addition of carbon black to the matrix decreases the creep compliance due to the significant interaction between the fiber and matrix, which leads to the increased modulus.

Table. 5. *Shear modulus G of EBC/CB composite at 0.01% shear strain*

CB content (wt.%)	Shear modulus G (MPa)
0	1.720 ± 0.08
10	7.414 ± 0.35
15	8.902 ± 0.38
20	13.670 ± 0.52
25	15.305 ± 0.71

The nanocomposites' mechanical properties were measured as a function of CB loading, and forces are shown in Figure 12.

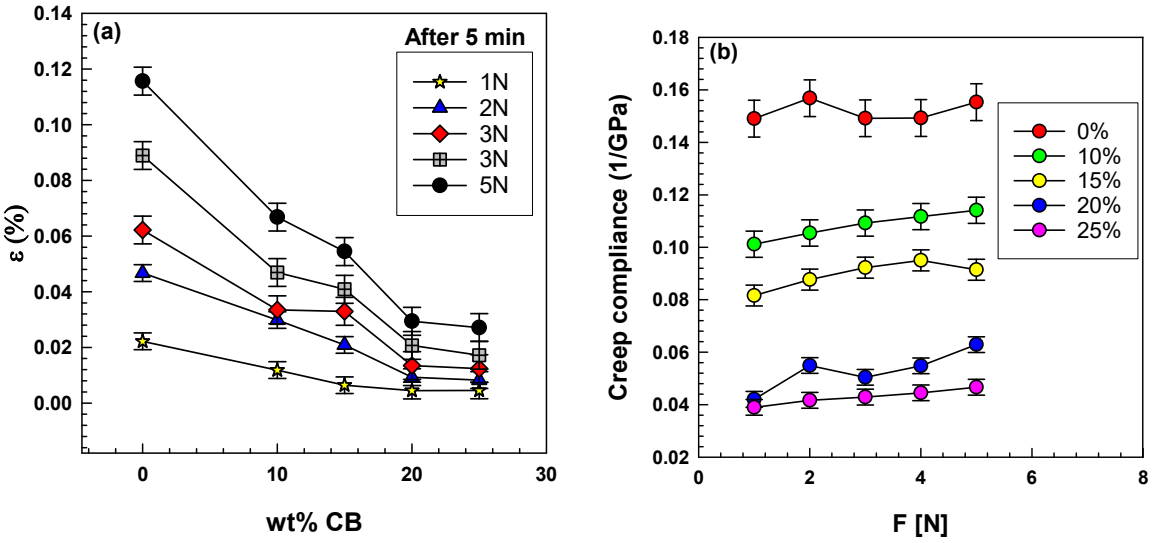

Fig. 12. a) Strain vs. CB concentration for different force after 5 min b) creep compliance vs. force for different loading of CB content.

Stress-strain tensile curves from DMA tests are shown in Figure 13. The Figure shows that the addition of CB from 0 wt.% to 25 wt.% to EBC would increase the modules Pa. Table 5 shows the modulus change by the addition of CB fiber at 0.01 as mathematical representations rely on the linearity of response of both elastic and viscous components. Moreover, it looks by increasing the fiber content. The copolymer composite tent to act more brittle. Stress-strain tensile curves from DMA tests are shown in Figure 24. The Figure shows that the addition of CB from 0 wt.% to 25 wt.% to EBC would increase the modules Pa. Table 6 shows the modulus change by the addition of CB fiber at 0.01 shear strain (27) as mathematical representations rely on the linearity of response of both elastic and viscous components. It shows that by increasing the CB content to the matrix, the Young modulus would increase from 7.414 for 10 wt.% Pa to 15.305 for 25 wt.%. Savetlana et al. reported that the addition of 20 wt.% carbon black to the natural rubber could increase the modulus for 18 times from 2.5 to 47 MPa because of the reinforcing potential from flexible filler formation network and strong polymer-filler coupling.

The principal factors determined the capability of reinforcement were (i) Van der walls force between CB and polymer, (ii) the chemical cross-link of polymer into the filler surface due to the free radical reaction between carbon atoms in filler and polymer, and (ii) the mechanical interlocking of the polymer on to the filler surface.(28) Moreover, it looks like increasing fiber content. The copolymer composite tend to acts more brittle, which might be because of the quality of the fibers dispersion and good interaction between carbon black and ethylene butene copolymer. This is the global result of an efficient load transfer from the matrix to the first, strong chemical interactions and second, geometric interactions, such as the

high specific surface area between the carbon black surface and the ethylene butane copolymer segments.(29-31) It has been established by numerous studies that addition of carbon base fibers exhibit a significant increase in modulus as compared to the matrix resin. As mentioned earlier, this is mainly due to the fact that functionalization improves both dispersion and stress transfer

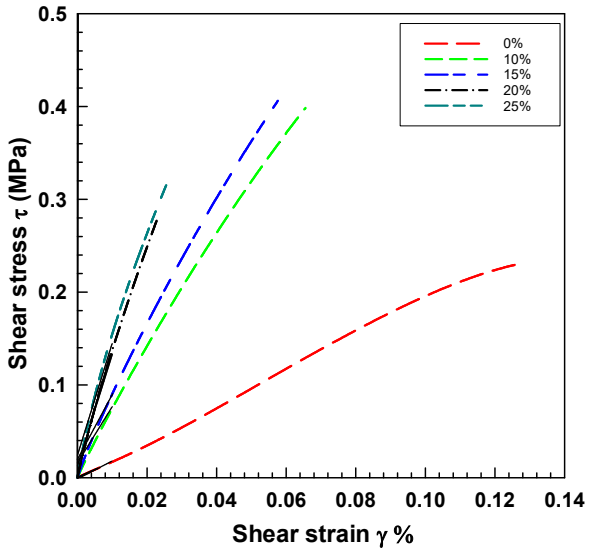

Fig. 13. Representative tensile stress-strain curves for EBC/CB for different concentrations.

The electric resistance vs. force is shown in Figure 14b. In this test, the electrical resistance was measured with a variety of loads for 5 min. However, the addition of CB up to 10 wt.% would not affect resistance. It might be related to the low concentration of carbon black in the matrix caused by disassociation between CB particles. That could decrease the resistance to almost zero. There are two types of electrical conduction in the EBC/CB that can happen. "Contact" or "tunneling" mechanism. Conductive fillers are physically in contact with each other and form a conducting network in the contact mechanism. However, the electron's mobility has tunneled between the neighboring conductive fillers, which are separated by the polymeric layers in the tunneling mechanism (32, 33).

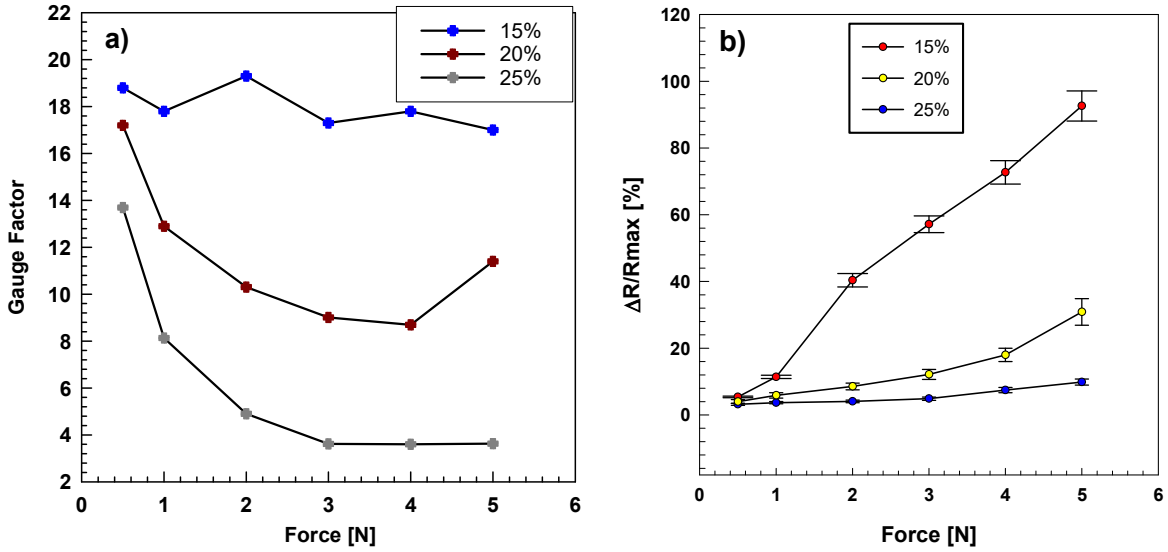

Fig. 14. A) Gauge factor b) Change of electrical resistance vs. force for different concentrations of CB.

Costa *et al*. (34) reported that the piezoresistive polymer blends gauge factor (GF) values ranging from 5 to 80. The gauge factor can be defined as (35, 36)

$$G = \frac{1}{\varepsilon}\left(\frac{\Delta R}{R_0}\right) \quad (2)$$

Where R_0 is initial resistance, ΔR is the change of resistance and ε is a strain. For a composite with strain-independent conductivity behavior, the following relationship is generally followed:(37)

$$\frac{\Delta R}{R_0} = \varepsilon\,(2 + \varepsilon\,) \quad (3)$$

Figure 14a indicates the gauge factor for different CB concentrations under force between 4 and 20, which is around five times higher than conventional metal gauge. It shows that the addition of CB to EBC could decrease the gauge factor with force.

The gauge factor is around two at low strain, but it may be as high as 1300 for carbon nanotube /epoxy composite (38). However, the most reported value is below 100 (34, 36, 39).

The addition of CB from 15 wt.% to 25 wt.% leads to an increase in the resistance dramatically, increasing interaction and contacting the CB particles. Moreover, increasing the force leads to a decrease in the thickness of the sample. It caused an increase in the interaction of CB particles.

Storage modulus (G′) and loss modulus (G″) was tested as a function of shear strain (γ %).

In the frequency sweep test, a small amplitude oscillatory shear, $\dot{\gamma} = \gamma_o \sin(\omega t)$ was applied to the samples. Resulting shear stress was recorded as:

$$\sigma(t) = \gamma_o[G'(\omega)\sin(\omega t) + [G''(\omega)\cos(\omega t)] \quad (4)$$

G′, G″ and dynamic viscosity (η∗) were measured as a function of angular frequency (ω) in the range of 0.01–100 rad/s at a strain value in the linear viscoelastic region (40, 41).

Figure 15 indicates the storage modulus (G') and loss modulus (G'), Tan δ, and complex viscosity $|\eta^*|$ of the samples as a frequency function.

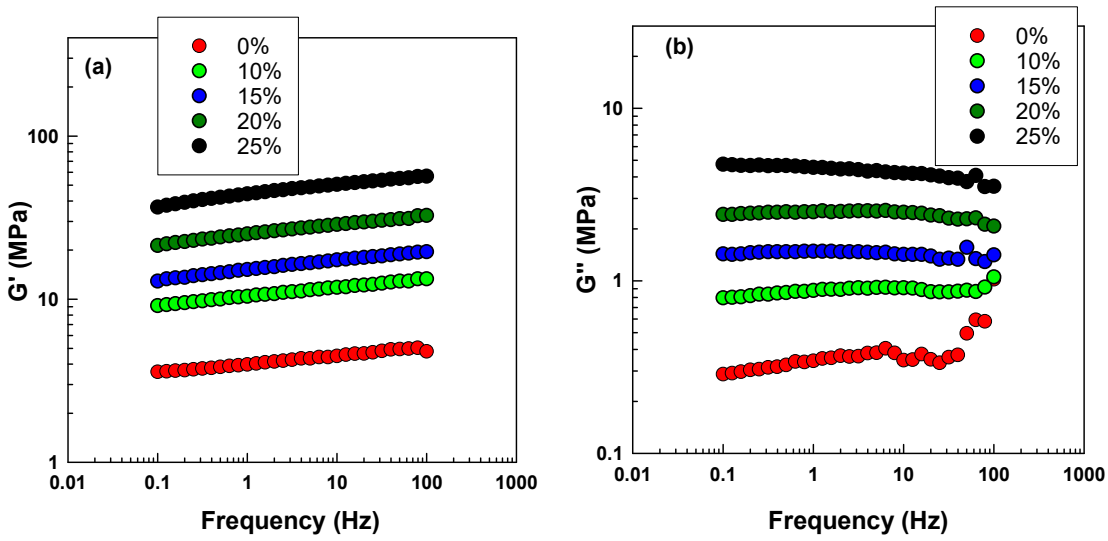

Fig. 15. (a) G', (b) G", as a function of frequency composites for different CB content for EBC/CB

It is observed that the loose modulus (G') is more sensitive than G". It is well known that the storage modulus with the changes of CB content.

There is no significant change in storage modulus observed for EBC/CB up to 20 percent because there is no interfacial interaction between CB fiber and EBC. However, EBC with 25 wt.%. Content will decrease the storage modulus up to 30% from 5 to 3.5 MPa for the entire frequency rate.

On the other hand, it can be observed that G' is increased significantly by increasing the frequency. It also can be observed that the addition of CB up to 25 wt.% could increase G' up to 3 times.

Dependence of loss factor (tan δ) and complex viscosity $|\eta^*|$ of the samples on frequency are given in Figure 16. Tan δ curves of the polymer copolymer with CB decreased with increasing frequency.

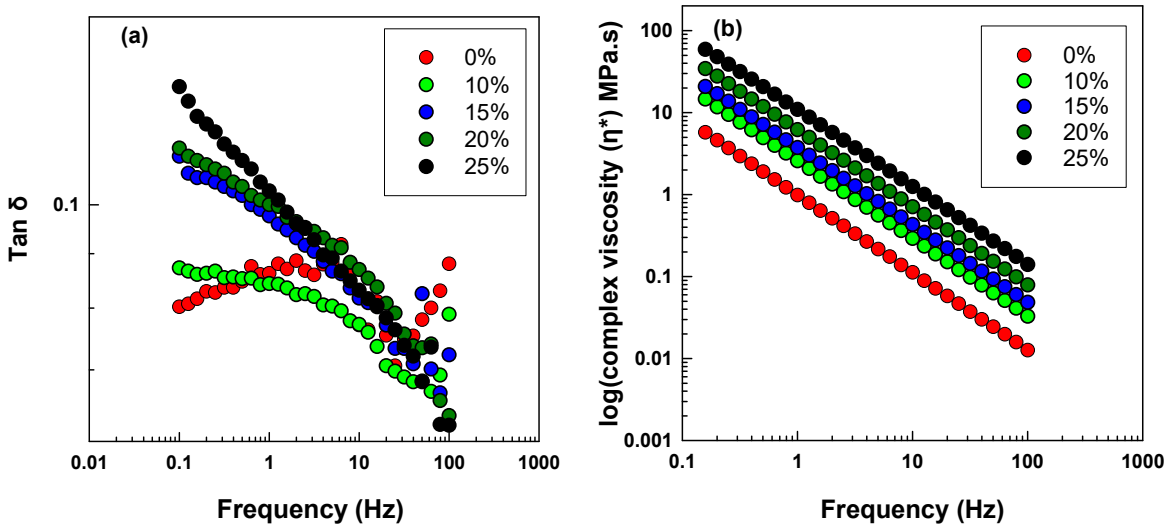

Fig. 16. (a) tan δ (b) |η| as a function of frequency composites for different CB content for EBC/CB*

The negative slope in the Tan δ curve is a normal behavior of viscoelastic. In contrast, the positive slope refers to the elastic response of the viscoelastic samples dominating this elastic behavior.

$$\tan\delta = \frac{G''}{G'}\ Eq \quad (5)$$

Figure 16b. $|\eta^*|$ curves with frequency region were fitted by the power-law model to determine the shear-thinning phenomena.

The dynamic viscosity is calculated according to equation 6.

$$|\eta^*| = k\omega^n \quad (6)$$

$$log|\eta^*| = \log k + n\log(\omega) \quad (7)$$

The shear-thinning exponent, n, is the straight-line slope obtained by plotting log |η*|vs. log ω (42-44).

The volume fraction of the carbon black (Φ) is calculated according to equation 8.

$$\phi = \frac{V_A}{V_A + V_B} = \frac{\frac{m_A}{\varrho_A}}{\frac{m_A}{\varrho_A} + \frac{m_B}{\varrho_B}} = \frac{\frac{m_A}{\varrho_A \cdot (m_A + m_B)}}{\frac{m_A}{\varrho_A \cdot (m_A + m_B)} + \frac{m_A}{\varrho_A \cdot (m_A + m_B)}}$$

$$= \frac{\frac{w_A}{\varrho_A}}{\frac{w_A}{\varrho_A} + \frac{w_B}{\varrho_B}} \quad (8)$$

While the density of CB and EBC is 0.125 g/cm^3 and 0.862 g/cm^3, respectively. The volume fraction is shown in Table 7.

The van Gurp-Palmen (vGP) plot, which plots phase angle δ° versus complex modulus |G*|, is sensitive to polydispersity and long-chain branching (95, 96).

The complex modulus |G*| is reported:

$$"|G^*| = (G'^2 + G''^2)^{1/2} \quad (9)$$

Table. 6. Power-law factors determined from the |η*|vs log ω

ϕ% CB	Composite Density g/cm^3	k	ω
0	0.862	-0.1951 ± 0.087	-0.9483
4.07	0.92	0.2199 ± 0.0103	-0.9457
6.31	0.95	0.3824 ± 0.0183	-0.9418
8.71	0.98	0.6007 ± 0.0284	-0.9416
11.28	1.02	0.8441 ± 0.0325	-0.9396

As shown in Figure 17, van Gurp-Palmen curves of EBC/CB show that the addition of CB to the EBC would increase. The blend shows the vGP plot predicted for linear polymers, i.e., a plateau at b = 7° in the low IG*I region.

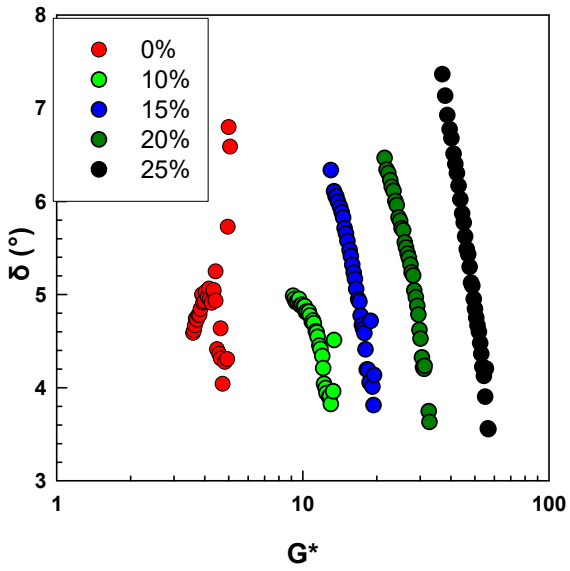

Fig. 17 vGP of EBC for different CB content

The graphs show that addition CB content could increase δ ̊from 3.5° to 7°. Several studies have been reported about vGP, which have been similar tend peak followed by a downward tendency (45-48).

5. Influence of Carbon fiber on ethylene butene copolymer (EBC)

The electrical, mechanical, and thermal conductivity of ethylene butene copolymer (EBC) composites with carbon fibers were studied. EBC/carbon-fiber composites can be utilized as an electromechanical material capable of changing its electric resistance with mechanical strain. Carbon fibers were introduced to EBC with different concentrations (5-25 wt. %).

Electrical conductivity

Tensile deformation and gauge factors were determined by a two-point technique to measure the electric resistance as a function of the strain. The composite samples with the various CF (5, 10, 15, 20 and 25 wt. %) were deformed by the tensile stress with increasing values of stress (0.442, 0.884, 1.325, and 1.768, and 2.219 MPa) respectively. Micrograph of optical microscopy from EBC carbon fiber for 15 wt. % and 25 wt. % can be seen in Figure 18.

Figure 18 shows the fracture morphologies of EBC with 15 wt. % and 25 wt.% of carbon fiber. The optical microscopy examination indicated that the fibers were homogeneously distributed in the EBC composites. It was also observed that at low fiber contents, 15 wt.%, fewer fibers were lying on the surface in comparison with the 25 wt.% carbon fiber

The composite with 25 wt.% carbon fiber had higher fiber agglomerates because of low dispersion caused by excess filler (100).

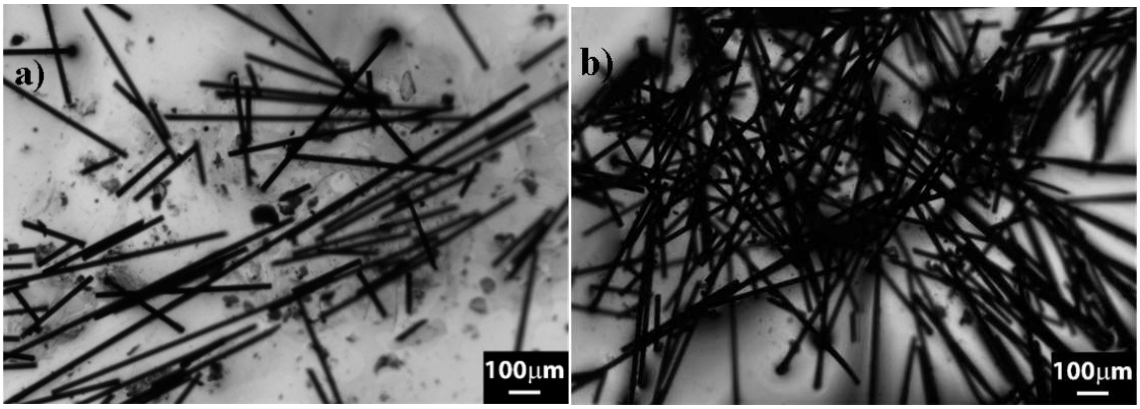

Fig. 18. Micrographs from optical microscopy (a) ethylene-butene -copolymer (EBC) and carbon fiber (CF) with 15 wt.% (b) ethylene-butene copolymer (EBC) and carbon fiber (CF) 25 wt.%.

. The strain caused by tensile stress, and the change of electrical resistance was measured. The change of electric resistance of EBC with 5% and 10% of carbon fibers could not be measured. There being zero conductivity because of the low concentration of CF. It was also observed that the EBC composite with 15% of carbon fiber had a low chance of electrical resistance with a change of strain due to the low content of carbon fibers, which might be because of the lower amount of fiber and resistivity of carbon fiber during the deformation. Furthermore, it is observed in Figure 3 that EBC/CF with 25 wt. % resistance change is increasing with deformation, as increasing the connection between carbon fibers.(1, 49, 50). The number of fibers in EBC/CF 15 wt. % is much lower than 25 wt.% that could be measured only up to 0.884 MP. The Figure shows that five cycles increase of tensile strain up to 2.935 MPa for 25 wt. % and four steps up to 1.768 MPa for 15 wt. % of CF.

By opening the circles in the graph, the relevant resistance changes while the values of strain are signified by solid circles. Figure 19 shows that EBC/CF 25 wt. % is conductive at the peak strain of about 16% once the resistance change is about 4500%.

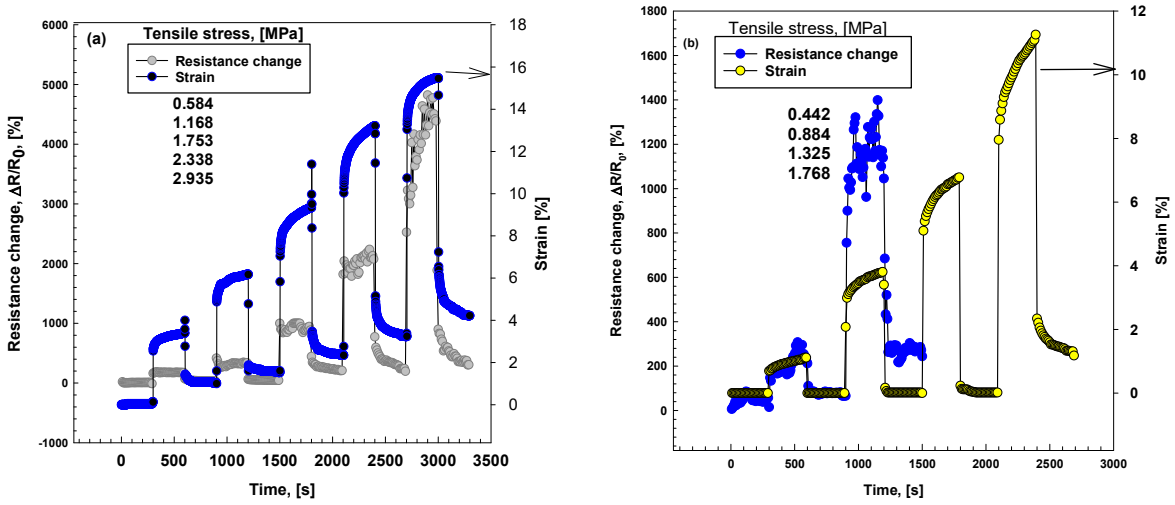

Fig. 19. Relative resistance change, $\Delta R/R_0$, and the strain, ε, of a) EBC/CF 25 wt.% b) EBC/CF 15 wt.%.

The relative resistance increases with strain continually with no gap. It is no longer common in the conductive particulate mixture when a point of very high resistance is touched the higher strain. Furthermore, the mixtures' resistance returns almost to unload state to the value of 0 and 3 percent for 15 wt. % and 25 wt. %, respectively, as can see in Figure 20.

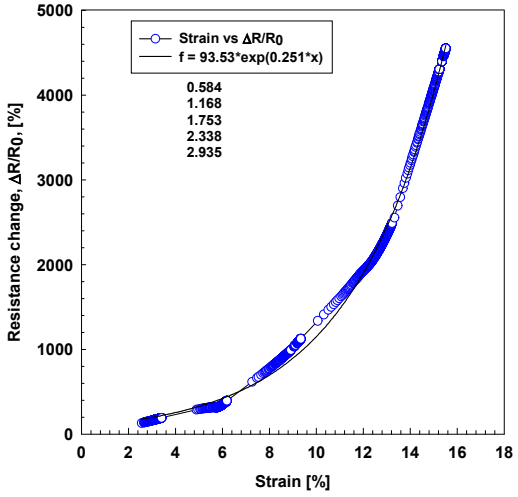

Fig. 20. Resistance change vs. strain for EBC/CF 25 wt. % composite in loading/unloading

Figure 21 indicates the gauge factor for EBC/CF 25 wt. %. The gauge factor rises with strain values around 50 and at starting of deformation and growth as much as 300 at a 16% strain. This is a remarkable growth that keeps EBC/CF mixture within the variety of mixture of substances and strain gauges with excellent sensitivity to tensile deformation.

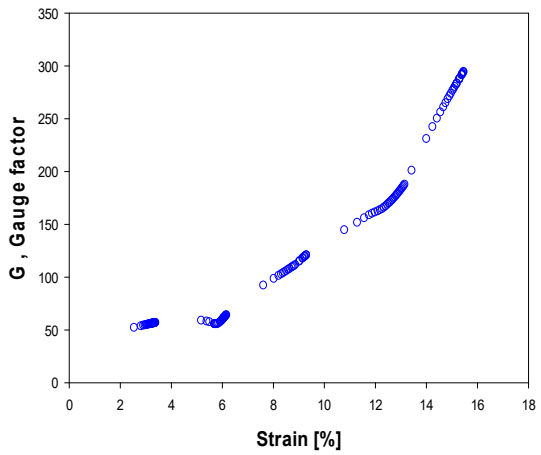

Fig. 21 Strain dependence of gauge factor GF of EBC/CF 25 wt. %

Thermal conductivity

The dependence of temperature on time is described with the equation 11.(51)

$$T = T_1 - (T_1 - T_2) * e^{|-(A_1 - A_2)\tau|} \quad (10)$$

Where:

$$A_1 = \frac{S\lambda}{\delta K} \, , A_2 = \frac{B}{K} \qquad (11)$$

However, equation 11 can be simplified with exponential growth with three parameters as:

$$y = y_0 + ae^{(-bx)} \qquad (12)$$

The coefficient b is obtained from the nonlinear regression. The calculation of the thermal conductivities of EBC/CF is shown in Table 7 and Figure 22.

Table. 7. The thermal conductivity Parameters of EBC/CF

CF wt.%	b	A1	λ (W m^{-2} K^{-1})	R^2
0	0.0015611	0.0012981	0.1952	0.999976
5	0.0019353	0.0016723	0.2266	0.999961
10	0.0020541	0.00179114	0.2413	0.999968
15	0.0021213	0.00185826	0.2477	0.999968
20	0.0023160	0.002053	0.2635	0.999979

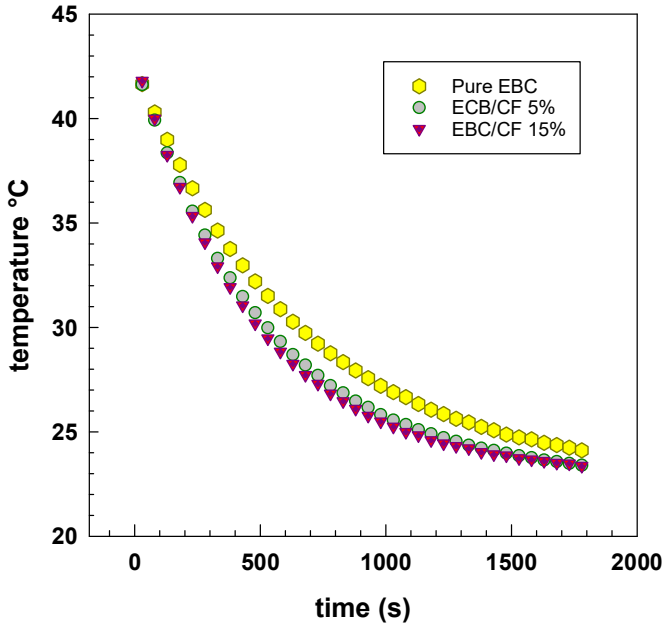

Fig. 22. Thermal conductivity measurement: temperature vs. time for EBC/CF for different concentration of carbon fiber content with the initial temperature of 45°C

Figure 23 shows that the thermal conductivities of the EBC/CF composites increased with increasing CF.

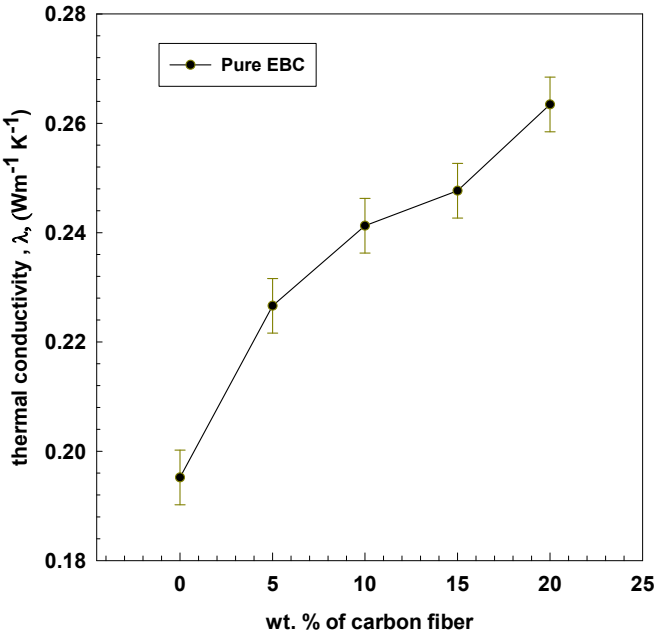

Fig. 23. Thermal conductivity as a function of the carbon fiber content

The highest measured thermal conductivity was 0.263 W m^{-1} K^{-1} for an EBC/CF 20 wt.% increase of 35% compared with pure EBC.

The uniform distribution of CF had a large effect on the growth in thermal and electric conductivity. Since CF has high conductivity for both heat and electricity, the CF loading in EBC resulted in an increase in the mixture's thermal and electric conductivities (51, 52).

6. Conclusions

The influence of carbon fibers and radiation on shear stress creep compliance and frequency sweep of ethylene-vinyl acetate (EVA) was investigated by dynamic mechanical analysis. The linear viscosity and electromechanical properties of Ethylene Butene copolymers filled with electric conductive Carbon Black and Carbon fiber are investigated.

Ethylene-vinyl acetate and Ethylene butyl copolymer with carbon fiber were mixed and homogenized with different concentrations (5, 10, 15, 20, 25 wt.%) using a two-roll mill at 150 °C for 5 min. Following, a sheet with a thickness of 0.5 mm was prepared by compression moldings at 10 MPa with 5 min. The same process is performed for Ethylene butyl copolymer and carbon black.

The EVA-CF composites were found to have higher shear modulus for given shear strain by adding filler and increasing irradiation due to the interaction between the matrix and fiber and increasing the molecular weight irradiation due to cross-linking. It was also observed that tan δ decreased with increasing doses from 60 to 180 kGy for 0.1 to 100 Hz frequencies. There was a dramatic decrease in creep with increasing CF content and increasing irradiation, which confirmed the high interaction and raised cross-linking level. The analysis of unsolvable gel content confirmed the effect of irradiation on cross-linking since the radiation dose up to 180 kGy increased the amount of insoluble gel.

The linear viscosity and electromechanical properties of Ethylene Butene copolymers filled with electric conductive carbon Black are investigated. The dynamic mechanical viscosity and modulus found to be increased with the addition of Carbon Black into Ethylene Butene copolymer. Moreover, the electrical resistance is growing with Carbon Black content due to the interaction and contact between the particles. The elongation (ε) significantly decreases by increasing the CB content regarding the well disperses and hardening effect of CB.

These work results establish the potential of manufacturing flexible strain sensors using an economical and multipurpose method, with potential applications in flexible electronics products.

The observations from optical microscopy indicated a relatively good dispersion of carbon fiber in the matrix. The electromechanical testing showed that straining of

the composite led to a change of its macroscopic electrical resistance. The EBC/CF strain sensitive composites were relatively sensitive to strain, and the changes were reversible. Therefore, the results indicate the composites' good potential to be used as an electrical sensor for strain. The thermal conductivity of the mixtures indicated an increase in thermal conductivity with loading carbon fiber.

References:

1. Slobodian P, Riha P, Olejnik R, Matyas J, Machovsky M. Pre-Strain Stimulation of Electro-Mechanical Sensitivity of Carbon Nanotube Network/Polyurethane Composites. Ieee Sens J. 2016;16(15):5898-903.

2. Esmaeeli R, Aliniagerdroudbari H, Hashemi SR, Jbr C, Farhad S. Designing a New Dynamic Mechanical Analysis (DMA) System for Testing Viscoelastic Materials at High Frequencies. Modelling and Simulation in Engineering. 2019;2019:7026267.

3. Loh K, Nagarajaiah S. Innovative developments of advanced multifunctional nanocomposites in civil and structural engineering: Woodhead Publishing; 2016.

4. Das A, Stockelhuber KW, Jurk R, Saphiannikova M, Fritzsche J, Lorenz H, et al. Modified and unmodified multiwalled carbon nanotubes in high performance solution-styrene-butadiene and butadiene rubber blends. Polymer. 2008;49(24):5276-83.

5. Yu KJ, Wang ML, Wu JQ, Qian K, Sun J, Lu XF. Modification of the Interfacial Interaction between Carbon Fiber and Epoxy with Carbon Hybrid Materials. Nanomaterials-Basel. 2016;6(5).

6. Hamid Y, Abu Bakar A, Deirram N. Mechanical and Morphological Properties of Waste Eurycoma longifolia Fiber/Montmorillonite Reinforced Poly(vinyl chloride) Hybrid Composites. J Appl Polym Sci. 2013;128(2):1170-5.

7. Potschke P, Fornes TD, Paul DR. Rheological behavior of multiwalled carbon nanotube/polycarbonate composites. Polymer. 2002;43(11):3247-55.

8. Poongavalappil S, Svoboda P, Theravalappil R, Svobodova D, Danek M, Zatloukal M. Study on the influence of electron beam irradiation on the thermal, mechanical, and rheological properties of ethylene-octene copolymer with high comonomer content. J Appl Polym Sci. 2013;128(5):3026-33.

9. Mandal S, Alam S. Studies on the mechanical, thermal, and morphological properties of poly(ether ether ketone)/poly(ether sulfone)/barium titanate nanocomposites: Correlation of experimental results with theoretical predictive models. J Appl Polym Sci. 2012;126(2):724-33.

10. Oliani WL, Lima LFCP, Parra DF, Dias DB, Lugao AB. Study of the morphology, thermal and mechanical properties of irradiated isotactic polypropylene films. Radiat Phys Chem. 2010;79(3):325-8.

11. Matthews KH, Stevens HNE, Auffret AD, Humphrey MJ, Eccleston GM. Gamma-irradiation of lyophilised wound healing wafers. Int J Pharm. 2006;313(1-2):78-86.

12. Rezaeian I, Jafari SH, Zahedi P, Ghaffari M, Afradian S. Improvements of physical and mechanical properties of electron beam irradiation-crosslinked EVA foams. Polym Advan Technol. 2009;20(5):487-92.

13. Matsui T, Shimoda M, Osajima Y. Mechanical Changes of Electron-Beam Irradiated Ethylene Vinyl-Acetate Copolymer (Eva) Film .1. Polym Int. 1992;29(2):85-90.

14. Shokrieh Z, Shokrieh MM, Zhao Z. A modified micromechanical model to predict the creep modulus of polymeric nanocomposites. Polym Test. 2018;65:414-9.

15. Svoboda P, Svobodova D, Mokrejs P, Vasek V, Jantanasakulwong K, Ougizawa T, et al. Electron beam crosslinking of ethylene-octene copolymers. Polymer. 2015;81:119-28.

16. Theravalappil R, Svoboda P, Poongavalappil S, Svobodova D. Creep and Dynamic Mechanical Analysis Studies of Peroxide-Crosslinked Ethylene-Octene Copolymer. Macromol Mater Eng. 2012;297(8):761-7.

17. Poongavalappil S, Svoboda P, Theravalappil R, Svobodova D, Vasek V, Jantanasakulwong K, et al. Cross-linking kinetics study and high temperature mechanical properties of ethylene-octene copolymer (EOC)/dicumylperoxide(DCP) system. Eur Polym J. 2011;47(10):1949-55.

18. McNally T, Potschke P, Halley P, Murphy M, Martin D, Bell SEJ, et al. Polyethylene multiwalled carbon nanotube composites. Polymer. 2005;46(19):8222-32.

19. Mussatti FG, Macosko CW. Rheology of Network Forming Systems. Polym Eng Sci. 1973;13(3):236-40.

20. Potschke P, Abdel-Goad M, Alig I, Dudkin S, Lellinger D. Rheological and dielectrical characterization of melt mixed polycarbonate-multiwalled carbon nanotube composites. Polymer. 2004;45(26):8863-70.

21. Kim H, Macosko CW. Processing-property relationships of polycarbonate/graphene composites. Polymer. 2009;50(15):3797-809.

22. Varghese AM, Rangaraj VM, Mun SC, Macosko CW, Mittal V. Effect of Graphene on Polypropylene/Maleic Anhydride-graft-Ethylene Vinyl Acetate (PP/EVA-g-MA) Blend: Mechanical, Thermal, Morphological, and Rheological Properties. Ind Eng Chem Res. 2018;57(23):7834-45.

23. Turgis JD, Coqueret X. Electron beam sensitivity of butyl acrylate copolymers: effects of composition on reactivity. Macromol Chem Physic. 1999;200(3):652-60.

24. Svoboda P. Influence of Branching Density in Ethylene-Octene Copolymers on Electron Beam Crosslinkability. Polymers-Basel. 2015;7(12):2522-34.

25. Sharif J, Aziz SHSA, Hashim K. Radiation effects on LDPE/EVA blends. Radiat Phys Chem. 2000;58(2):191-5.

26. Svoboda P. High-temperature study of radiation cross-linked ethylene-octene copolymers. Polymer Bulletin. 2017;74(1):121-44.

27. Capela C, Oliveira S, Ferreira J. Mechanical behavior of high dosage short carbon fiber reinforced epoxy composites. Fibers and Polymers. 2017;18(6):1200-7.

28. Savetlana S, Zulhendri, Sukmana I, Saputra FA. The effect of carbon black loading and structure on tensile property of natural rubber composite. IOP Conference Series: Materials Science and Engineering. 2017;223:012009.

29. Hamid Y, Bakar AA, Deirram N. Mechanical and morphological properties of waste Eurycoma longifolia fiber/montmorillonite reinforced poly (vinyl chloride) hybrid composites. J Appl Polym Sci. 2013;128(2):1170-5.

30. Hamid Y, Svoboda P, Svobodova D. Influence of Electron Beam Irradiation on High-Temperature Mechanical Properties of Ethylene Vinyl Acetate/Carbon Fibers Composites. Journal of Vinyl and Additive Technology. 2020;26(3):325-35.

31. Le T-T. Prediction of tensile strength of polymer carbon nanotube composites using practical machine learning method. J Compos Mater. 2020:0021998320953540.

32. Varghese AM, Rangaraj VM, Mun SC, Macosko CW, Mittal V. Effect of Graphene on Polypropylene/Maleic Anhydride-graft-Ethylene–Vinyl Acetate (PP/EVA-g-MA) Blend: Mechanical, Thermal, Morphological, and Rheological Properties. Ind Eng Chem Res. 2018;57(23):7834-45.

33. Yousefi N, Sun X, Lin X, Shen X, Jia J, Zhang B, et al. Highly aligned graphene/polymer nanocomposites with excellent dielectric properties for high-performance electromagnetic interference shielding. Adv Mater. 2014;26(31):5480-7.

34. Costa P, Oliveira J, Horta-Romarís L, Abad M-J, Moreira JA, Zapiráin I, et al. Piezoresistive polymer blends for electromechanical sensor applications. Compos Sci Technol. 2018;168:353-62.

35. Biccai S, Boland CS, O'Driscoll DP, Harvey A, Gabbett C, O'Suilleabhain DR, et al. Negative gauge factor piezoresistive composites based on polymers filled with MoS2 nanosheets. Acs Nano. 2019.

36. Bhandari S. Polymer/Carbon Composites for Sensor Application. In: Rahaman M, Khastgir D, Aldalbahi AK, editors. Carbon-Containing Polymer Composites. Singapore: Springer Singapore; 2019. p. 503-31.

37. Chen S, Lou Z, Chen D, Jiang K, Shen G. Polymer-Enhanced Highly Stretchable Conductive Fiber Strain Sensor Used for Electronic Data Gloves. Adv Mater Technol-Us. 2016;1(7):1600136.

38. Anand SV, Mahapatra DR. Quasi-static and dynamic strain sensing using carbon nanotube/epoxy nanocomposite thin films. Smart Mater Struct. 2009;18(4):045013.

39. Zhou J, Hsieh Y-L. Conductive Polymer Protonated Nanocellulose Aerogels for Tunable and Linearly Responsive Strain Sensors. Acs Appl Mater Inter. 2018;10(33):27902-10.

40. Adefisan OO, McDonald AG. Evaluation of the strength, sorption and thermal properties of bamboo plastic composites. Maderas Ciencia y tecnología. 2019;21(1):3-14.

41. Arulmurugan M, Prabu K, Rajamurugan G, Selvakumar A. Impact of BaSO 4 filler on woven Aloevera/Hemp hybrid composite: Dynamic mechanical analysis. Mater Res Express. 2019.

42. Durmuş A, Woo M, Kaşgöz A, Macosko CW, Tsapatsis M. Intercalated linear low density polyethylene (LLDPE)/clay nanocomposites prepared with oxidized polyethylene

as a new type compatibilizer: Structural, mechanical and barrier properties. Eur Polym J. 2007;43(9):3737-49.

43. Durmus A, Kasgoz A, Macosko CW. Linear low density polyethylene (LLDPE)/clay nanocomposites. Part I: Structural characterization and quantifying clay dispersion by melt rheology. Polymer. 2007;48(15):4492-502.

44. Mussatti FG, Macosko CW. Rheology of network forming systems. Polymer Engineering & Science. 1973;13(3):236-40.

45. López-Barrón C, Macosko C. Rheology of compatibilized immiscible blends with droplet-matrix and cocontinuous morphologies during coarsening2014. 1935-53 p.

46. Trinkle S, Walter P, Friedrich C. Van Gurp-Palmen Plot II – classification of long chain branched polymers by their topology. Rheol Acta. 2002;41(1):103-13.

47. Rulduà MLM, Raquez J, Re G, Santana O, Dubois P, Cailloux J. Procesado en fundido de PLA reforzado con nanofibras de celulosa a partir de un masterbatch preparado de forma sostenible. Materiales Compuestos. 2019;3(3):107-11.

48. Delgado DE, Sturdy LF, Burkhart CW, Shull KR. Validation of quartz crystal rheometry in the megahertz frequency regime. Journal of Polymer Science Part B: Polymer Physics. 2019.

49. Slobodian P, Olejnik R, Matyas J, Babar DG, editors. Improving sensitivity of the polyurethane/CNT laminate strain sensor by controlled mechanical preload. IOP Conference Series: Materials Science and Engineering; 2016: IOP Publishing.

50. Slobodian P, Riha P, Olejnik R, Cvelbar U, Saha P. Enhancing effect of KMnO4 oxidation of carbon nanotubes network embedded in elastic polyurethane on overall electro-mechanical properties of composite. Composites Science and Technology. 2013;81:54-60.

51. Svoboda P, Theravalappil R, Poongavalappil S, Vilcakova J, Svobodova D, Mokrejs P, et al. A study on electrical and thermal conductivities of ethylene–octene copolymer/expandable graphite composites. Polymer Engineering & Science. 2012;52(6):1241-9.

52. Ren L, Li Q, Lu J, Zeng X, Sun R, Wu J, et al. Enhanced thermal conductivity for Ag-deposited alumina sphere/epoxy resin composites through manipulating interfacial thermal resistance. Composites Part A: Applied Science and Manufacturing. 2018;107:561-9.

Acknowledgement

These works has been supported by the Internal Grant Agency (IGA/FT/2017/007) of the Tomas Bata University in Zlin)

Cross-linking, morphology and properties in polymer blends and composites

Síťování, morfologie a vlastnosti polymerních směsí a kompozitů

Doctoral Thesis Summary

Published by: Tomas Bata University in Zlín,

nám. T. G. Masaryka 5555, 760 01 Zlín.

Edition: published electronically

Typesetting by: Yasin Hamid Ph.D.

This publication has not undergone any proofreading or editorial review.

Publication year: 2021

First Edition

ISBN 978-80-7454-998-4